We would like to thank the Editor and the three Reviewers for the time spent on our manuscript. Their comments and suggestions are considered in our revised version, which is largely improved thanks to their recommendations. Our point-to-point response is reported below. Reviewer's Comments are reproduced in italics; the Authors' Responses are given directly afterward. All reviewer comments are identified using the code *RXCY*, where *X* is the reviewer number and *Y* is the reviewer comment number (for example *R1C3* means Reviewer 1 Comment 3). Line numbers in authors' responses refer to the original manuscript unless otherwise stated. A marked-up manuscript follows after the response.

Reviewer 1 Massimiliano Zappa

Main Comments

R1C1: *"LUMPED or SEMI DISTRIBUTED. Here is the definition of lumped very broad and actually the implementation with elevation bands and radiation index classes heavily reminds me the definition of hydrological response units, also a semi-distributed approach. I think your approach is much more semi-distributed than lumped.*

In the manuscript, we characterised TOPMELT as 'lumped' in order to make very clear the differences with a spatially distributed approach. However, we agree with the Reviewer that the model can be considered as 'semi-distributed', as this class of models do not make calculations for every point in the catchment but for a distribution function of characteristics. TOPMELT has the feature that the snow predictions can be mapped back into space for comparison with any observations of the snow properties. We substituted 'lumped' with 'semi-distributed' in the revised version.

R1C2: *INPUT PRECIPITATION Please expand on the techniques declared at page 4*.

With the sentence at line 13, page 4, we mean that precipitation can be calculated by using a range of methods (Thiessen Polygons, multi-quadratic and Kriging), on the condition that the model input is an areal precipitation estimated starting from any of these techniques. The interpolation and averaging code of precipitation is not included in the version of TOPMELT illustrated in this manuscript, but it is included in the complete hydrological model code. For the case study of the paper, we used the Thiessen polygons to calculate an areal precipitation over the whole basin. We will clarify this issue in the revised version of the paper.

R1C3: *LIST OF VARIABLES I would welcome a Table with a list of the used abbreviations*.

A table with model parameters and variables is reported here below and is included in the revised version of the paper.

Table 1. Model parameters and variables: short name, description and measuring units. Parameters are written with capital letters, variables in lowercase.

Parameter	Description	Value	Units
$ALBG$	Glacier albedo	0.3	-
$ALBS$	Fresh snow albedo	0.9	-
β_2	Dimensionless parameter for alb computation	0.0919	-
CMF	Combined Melt Factor	0.013	mm $°C^{-1}MJ^{-1}m^2$
$DYTIME$	Speed of water propagation through snowpack	3	mh^{-1}
G	Precipitation gradient	0	km^{-1}
LWT	Water holding capacity, fraction of w.e.	0.1	-
NMF	Night Melt Factor	0.16	mm $°C^{-1}h^{-1}$
$REFRZ$	Freezing factor	0.03	mm $°C^{-1}h^{-1}$
RI	Radiation Index, mean daily energy	$1 \div 42$	MJ $m^{-2}h^{-1}$
RMF	Rain Melt Factor	0.3	mm $°C^{-1}h^{-1}$
T_b	Base temperature	0.0	°C
T_c	Snow/rain threshold temperature	1.5	°C
$WETH$	Water equivalent minimum threshold before ice-melt	5	mm
Variable	**Description**		**Units**
alb	Snow albedo (accounting for aging)		-
h	Elevation		m
f	Fusion		mm h^{-1}
ice	Freezed water		mm
$liqw$	Interstitial melt water		mm
p	Precipitation		mm h^{-1}
T	Temperature		°C
we	Water Equivalent (w.e.)		mm

R1C4: *"DYNAMIC" RADIATION AREA AND INDEX: If you had static radiation regions instead of radiation classes you would not need the supplementary workaround for updating the states with a "migration". Can you better justify your choice, or, even better, compare your results to a version with static radiation sub areas selected using elevation, aspect and/or slope?*

TOPMELT accounts for the seasonality of sun declination and for the visible horizon, therefore including both the effects of the temporal variability of the incident radiation angle and of shadowing. This makes the spatial distribution of radiation variable over time, which requires the updating of the snow states and represents a key feature of the model.
The use of topographic variables, like aspect, elevation and slope as a surrogate for radiation is similarly subject to arbitrariness and lack of generality. For instance, during winter months in Norther Hemisphere, portions of north-facing slopes may remain shaded throughout the day due to the low angle of the sun. This causes snow on north-facing slopes to melt slower than on south-facing ones. The scenario is just the opposite for slopes in the Southern Hemisphere, where north-facing slopes receive more sunlight and are consequently warmer. Near the Equator, north- and south-facing slopes receive roughly the same amount of sunlight because the sun is almost directly overhead. At the Poles, north and south slopes tend to be either shrouded in darkness all winter long, or bathed in sunlight all summer long, with only slight variation between the slopes in spring

and fall. All this, shows that using radiation instead of topographic variables leads to a better generalization of model application and evaluation.

The paper already includes an analysis of the impact of decreasing the frequency of the snow state updating. This can be seen in Figure 8 of the submitted paper, left panel, which shows the impact of updating the radiation distribution at decreasing frequency. The frequency ranges from 1 week, which is chosen as the reference temporal aggregation, to 2 weeks, 4 weeks, 8 weeks and 12 weeks. Figure 1 below shows the scatter plots corresponding to the pixel-by-pixel comparison summarised in Figure 8 of the submitted paper, in terms of snow water equivalent (w.e.). The scatter reported in Figure 1 indicates that the impact of the decreasing frequency may have important consequences when the w.e. spatial distribution is sought.

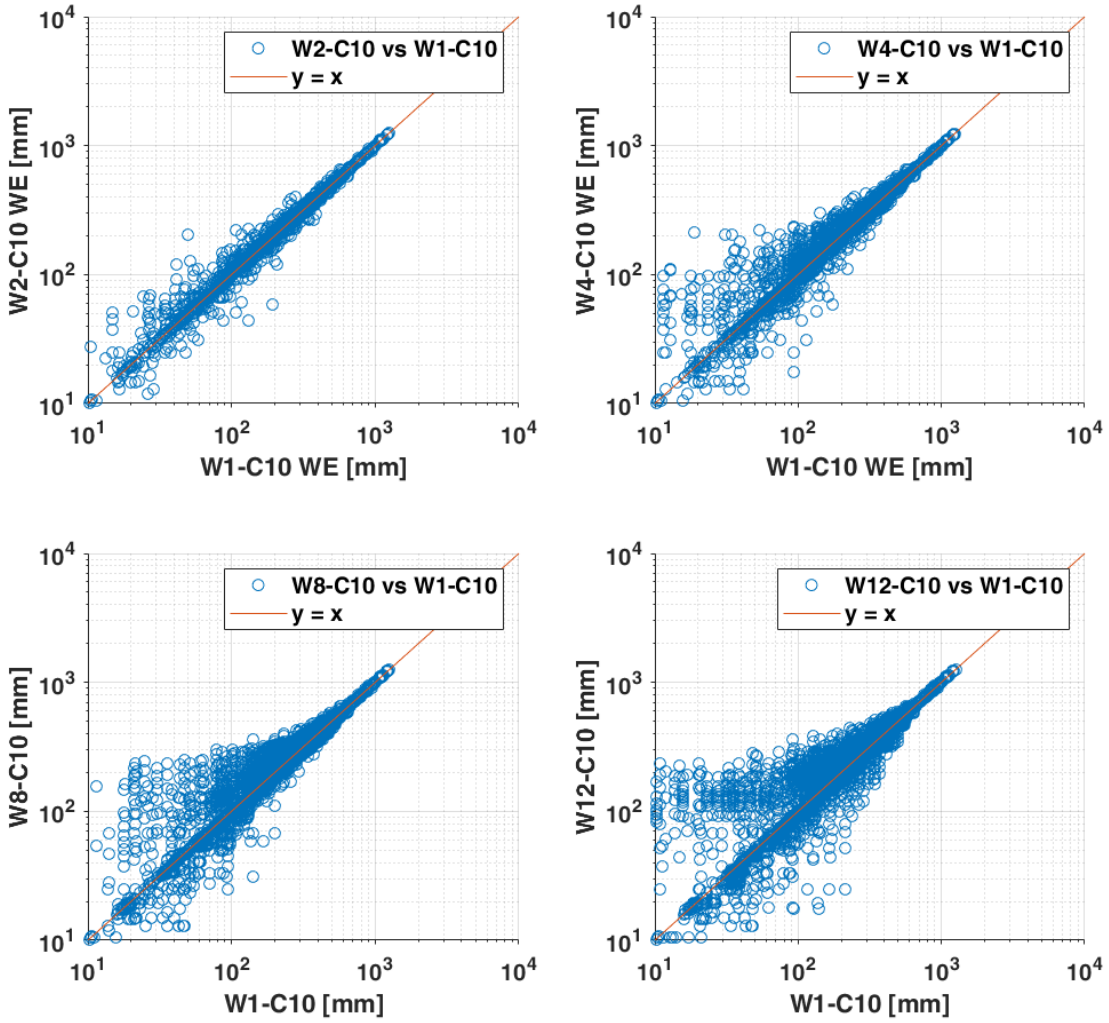

Fig. 1: Scatter plot of the pixel-by-pixel comparison of w.e., obtained by updating the w.e. classes at decreasing frequency ranging from 2 weeks to 12 weeks. The updating frequency of 1 week is used as reference. The study period is from October 1 2010 to June 30 2011.

Specific comments

R1C5: *Page 1, line 10: Similar topic was addressed in Klok et al, 2001, where Hock model has been implemented in a fully distributed and in a semi distributed model. Klok, L., K. Jasper, K. Roelofsma, A. Badoux, J. Gurtz (2001) Distributed hydrological modelling of a glaciated Alpine river basin. Hydrol. Sci. J. 46: 553-570.*
Reference added.

R1C6*: Page 1, line23: Zappa M, Pos F, Strasser U, Warmerdam P, Gurtz J. 2003. Seasonal water balance of an Alpine catchment as evaluated by different methods for spatially distributed snowmelt modelling. Nordic Hydrology 34: 179-202..*
Reference added.

R1C7: *Page 2, line 24: Here is the definition of lumped very broad and actually the implementation with elevation bands and radiation index classes heavily reminds me the definition of hydrological response units, also a semi-distributed approach..*

Please see our response to R1C1.

R1C8: *Page 2, line 28: A priori statement, not yet supported by results and/or references.*

The comment refers to the sentence: 'This is a potentially significant advantage when parameter sensitivity and uncertainty estimation procedures are carried out'. We have rephrased as follows: 'This is a potentially significant advantage when several model simulation runs should be carried out, such as in Monte Carlo based parameter sensitivity and uncertainty estimation procedures.'

R1C9: *Page 3, line 3: Making this a semi-distributed approach ....*

We agree on this comment, which underlines the need to term 'semi-distributed' the TOPMELT modelling approach.

R1C10: *Page 4, line 8: single for the whole basin and a specific day or single for the whole computation period?*

We thank the Reviewer for the opportunity to better specify here: 'Air temperature data are used to estimate an unique hourly vertical lapse rate for the whole basin' (revised Section 2.2, first paragraph).

R1C11: *Page 4, line 13: Reference(s)? This is the only place where you declare how P is interpolated, but it seems to me quite strange to declare a "range of techniques" used .... Did you use now Kriging or Thiessen?*

See our response to comment R1C2. We modified the original text as follows: 'The model permits use of several techniques ranging from Thiessen's polygons to multi-quadratic (Borga and

Vizzaccaro, 1997) for the estimation of basin mean areal precipitation values. For the analyses reported in this work, the Thiessen method was used' (revised Section 2.2, first paragraph).

R1C12: *Page 5, line 8: Rerference(s)?*

Reference was added (Anderson, 1976).

R1C12: *Page 5, line 10: A table provided as supplementary material listing all variable and units might be a good addon.*

Please see our response to R1C3

R1C13: *Figure 1: You define for each time and elevation band 10 sub-regions with equal area after sorting them according to RI. Why 10 areas? Why not discriminate them according to slope and aspect (which seems dominant to me).*

'Why 10 areas?' The impact of using different subdivisions is examined in Figure 8b of the submitted paper, where the number of classes ranges from 1 to 20, showing that the gain in reproducing the snow water equivalent spatial distribution is very limited when more than ten classes are used.

See our response to R1C4 for the comment concerning the use of topographic information to discriminate between local areas.

We revised the Figure 1 changing the colour scale (see below).

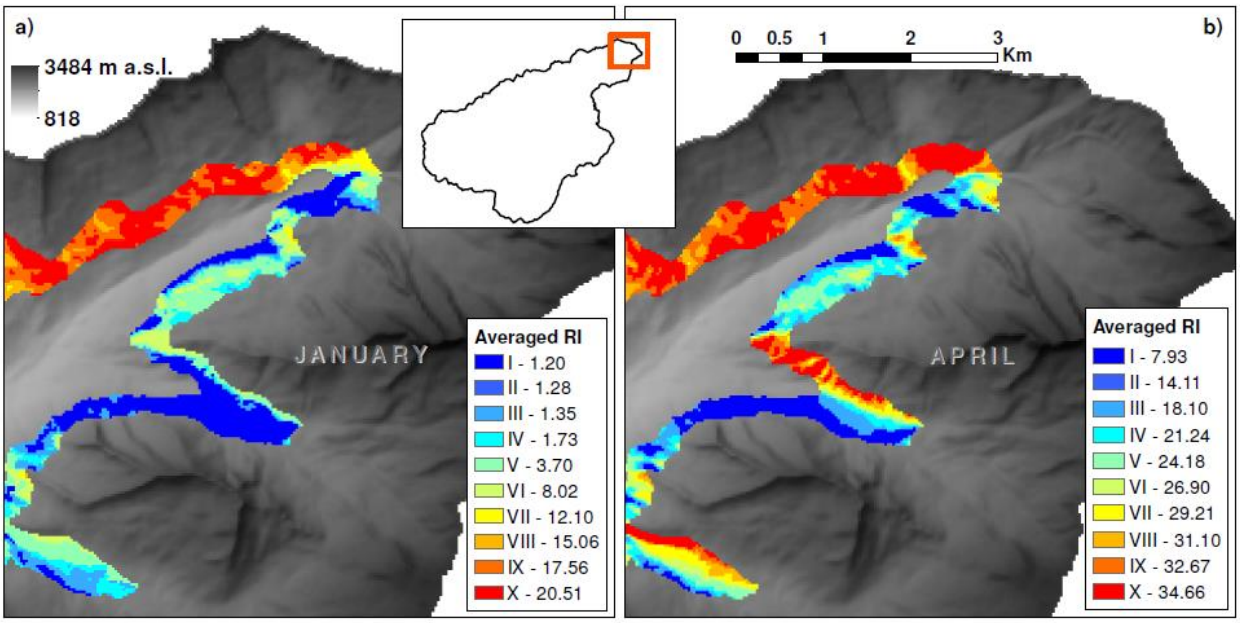

Figure 1. Comparison between radiation index distribution over the 2000-2200 m elevation band of the Aurino basin for a) January 1st and b) April 1st (ten classes subdivision). The figures show the north-eastern portion of the basin and report the average radiation index [J m^{-2}], with the corresponding radiation class identified by a roman number.

R1C14: *Page 6, line 14: If you had static radiation regions instead of radiation classes you would not need this supplementary workaround for updating the states. Can you better justify your choice, or, even better, compare you results to a version with static radiation sub areas selected using aspect and/or slope?*

See our response to R1C4 for the comment concerning the use of topographic information to discriminate between local areas.

R1C15: *Page 8, line 17: What is suitable in your opinion?*

We used 10 mm as a threshold value in this analysis. The revised version has been updated accordingly and a reference supporting the choice was added (Parajka and Blöschl, 2008).

R1C16: *Page 10, line 3: Thanks, this replies one of my previous points.*

Thanks

R1C17: *Page 10, line 20: For nc1 there should not be any migration, isn't?*

Yes, when using just one class there is no need to update the snow water equivalent.

R1C18: *Page 10, line 20: With static radiation classes you should not have any migration but exploiting the potential of ERI, isn't?*

The Reviewer is right in this remark, but we note that solar radiation is inherently variable in time. Thus, taking this variability into account should at least be attempted in a model which aims to use both temperature and radiation for snowmelt modelling.

R1C19: *Page 12, line 20: Zappa M. 2008. Objective quantitative spatial verification of distributed snow cover simulations – an experiment for entire Switzerland. Hydrological Sciences Journal, 53(1): 179–191. DOI: 10.1623/hysj.53.1.179.*

We added this reference.

R1C20: *Page 13, line 2: Still W4-C10?*

Yes, we put a note on this in the revised text.

R1C21: *Figure 6: I would be interested to see a "spaghetti plot" sorted by C and W.*

Whereas the sensitivity of the modelled snow water equivalent to variation of number of classes (C) and number of updates (W) is quite remarkable, the sensitivity of the modelled runoff is much less (actually, dispersion in the spaghetti plot cannot be recognised). This is due to the size of the study basin and the branching nature of the river network; both provide a powerful way in averaging out the heterogeneity of snowmelt processes, as shown by Comola et al. (2015). In order to illustrate this point, we reported values of the Nash-Sutcliffe index for different model simulations obtained

by using different values of C and W (see Table 2 of the revised paper, reported below). In the revised version, we also examined the control exerted by the catchment size on runoff simulations. We subdivided the study basin into a number of sub-basins characterised by different drainage areas. We isolated 5 basins with mean drainage of 20 km^2, 10 basins with mean drainage area of 10 km^2, and 20 basins with mean drainage area of 5 km^2. Results are reported in the new Section 3.4 of the revised version (see Table 3, reported below, for a summary).

Table 2. Nash-Sutcliffe index (NSE) of the TOPMELT-ICHYMOD model at different spatial aggregation and temporal resolution, from October 2001 to October 2007.

W4C1	**W4C5**	**W4C10**	**W4C15**	**W4C20**
0.73	0.73	0.71	0.73	0.73
W1C10	**W2C10**	**W4C10**	**W8C10**	**W12C10**
0.71	0.71	0.71	0.70	0.71

Table 3. Mean value of the Nash-Sutcliffe index (NSE) of the comparison between W4C1 and W4C10 TOPMELT-ICHYMOD simulated flows and the reference flow simulations, obtained by using the W4C20 set up, over basins of three different drainage areas: 5, 10 and 20 km^2. Comparisons carried out over the March. 1 to June, 30 period.

Model set-up	**Sub-basin area**		
	5 km^2	10 km^2	20 km^2
W4C1	0.77	0.91	0.99
W4C10	0.97	0.99	0.99

R1C22: *Figure 8: Why not using same scale of y-axis in the left and right graphs? So you could easily see that W is less sensitive than C*

In the revised version of the paper we used the same scale.

R1C23: *Page 15, line 5 (it is fig 8).*

Corrected.

Reviewer 2 Anonymous

Main Comments

R2C1: Page 4, line 14: The Precipitation Correction Factor is mentioned only here without further explanation or details. Is it an important parameter in the model? How is it determined? What are the typical values? In the revised manuscript, I suggest the authors to integrate the description of the Precipitation Correction Factor.

The Precipitation Correction Factor (PCF) accounts for poor estimation of the precipitation due to climatic non-representativeness of the gauging stations. Its value may be estimated by optimising the comparison statistics with snow cover MODIS data. In the specific application reported here, a value equal to 1.1 was used. Please note that since the corrected areal precipitation is an input to TOPMELT model, both PCF and SCF are not TOPMELT parameters.

R2C2: Page 8, line 17: How does the conversion snow-water equivalent maps to snow cover maps work? What are the 'suitable threshold values'? I suggest the authors to integrate the description in the text.

The comparison between model-based SWE and snow cover MODIS maps is carried out by converting the SWE map into a snow cover map using a threshold on SWE. In this paper, a minimum threshold of 10 mm was used. A reference (Parajka and Blöschl, 2008) and a brief note were added in section 4.3 of the revised paper. The revised paper is integrated with the following text:
'Then, the water equivalent maps may be converted to snow cover maps by using suitable threshold values (Parajka and Blöschl, 2008). In this work, we used a minimum threshold of 10 mm for the intercomparison with the MODIS snow cover products.'.

R2C3: Page 9, line 9: The authors should report the estimated fractions of catchment area for the different land uses. Does the model consider interception by various vegetation covers? If so, how? How does the snowmelt module work in forested areas and are there any differences compared to other land uses?

We thank the Reviewer for this note. The current version of the model does not consider land use for snow melt modelling. Accordingly, the model does not take into account neither interception of snow by the vegetation and reduction of solar radiation during melting periods. A version of the model which includes a simplified canopy model is already available, but it is not included in this work, where we focus on the basic elements of TOPMELT (use of statistical distribution of solar radiation and assessment of the impact of its different simplified representations).

R2C4: Page 13, lines 5-8: I think coniferous forests and discontinuous vegetation might be the dominant land covers in such a catchment. Therefore, given the limits of MODIS in vegetated areas, I suggest to show the comparison between TOPMELT and MODIS for all the land covers, except for the forested areas. As an alternative, the results of the comparison could be shown in a table or in the figures, but distinguishing the various land uses.
We thank the Reviewer for this note. As we reported in our Response to the comment R2C3, land use and impact of vegetation is not considered in this work. However, we recognise the limits of MODIS in vegetated areas. To account for this, the revised version includes a new version of Figure 7 (now Figure 6 in the revised version), where we report the land use distribution. The revised

version includes also text reporting the fractions of different land uses. This helps understanding the impact of forested areas on OA and better interpreting our results.

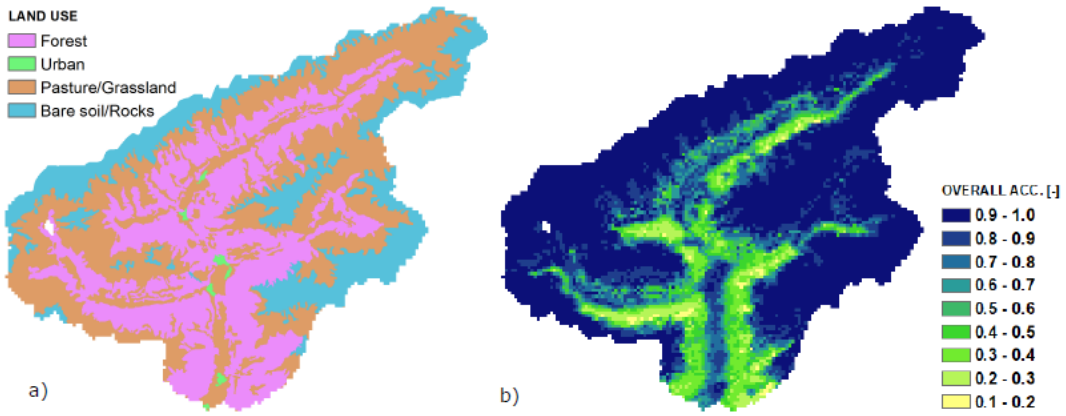

Figure 6. a) Land cover use for the catchment and b) pixel based overall accuracy (OA) of the comparison between simulated and MODIS-derived snow cover maps, computed from January 1 to June 30, 2011 for a total of 50 MODIS snow cover maps.

Minor comments

R2C5: *Page 2, line 16: Please revise the English in this sentence.*
Revised.

R2C6: *Page 3, line 23: It is not clear why the fraction of glacier area or debris-covered glacier area is mentioned here without further explanation. Please integrate here with 1-2 brief sentences.*
We removed any reference to the debris covered glacier to avoid unnecessary information, given that this feature was not used in the case study. We revised the text concerning the meaning of glacier area fraction.

R2C7: *Title 2.2: Does the model consider interception by different vegetation covers? And how?*
See R2C3 and R2C4

R2C8: *Page 4, Line 11: It is not clear what interpolation technique is used in the model. Please explain whether there are different options in the model. And please give more details about the Precipitation Correction Factor. How is it obtained/computed? What are the typical values?*
See R2C1. The paper was revised to better explain how the precipitation input is processed and passed to the model.

R2C9: *Eq 2: Maybe capital letters should be used here.*
In the revised paper we use capital letters for parameters and lowercase for variables, except for temperature *T*, which would confuse with time *t*. We added a table with variables and parameter definition (see Table 1 below).

Table 1. Model parameters and variables: short name, description and measuring units. Parameters are written with capital letters, variables in lowercase.

Parameter	Description	Value	Units
$ALBG$	Glacier albedo	0.3	-
$ALBS$	Fresh snow albedo	0.9	-
β_2	Dimensionless parameter for alb computation	0.0919	-
CMF	Combined Melt Factor	0.013	mm $°C^{-1}MJ^{-1}m^2$
$DYTIME$	Speed of water propagation through snowpack	3	mh^{-1}
G	Precipitation gradient	0	km^{-1}
LWT	Water holding capacity, fraction of w.e.	0.1	-
NMF	Night Melt Factor	0.16	mm $°C^{-1}h^{-1}$
$REFRZ$	Freezing factor	0.03	mm $°C^{-1}h^{-1}$
RI	Radiation Index, mean daily energy	$1 \div 42$	MJ $m^{-2}h^{-1}$
RMF	Rain Melt Factor	0.3	mm $°C^{-1}h^{-1}$
T_b	Base temperature	0.0	°C
T_c	Snow/rain threshold temperature	1.5	°C
$WETH$	Water equivalent minimum threshold before ice-melt	5	mm
Variable	**Description**		**Units**
alb	Snow albedo (accounting for aging)		-
h	Elevation		m
f	Fusion		mm h^{-1}
ice	Freezed water		mm
$liqw$	Interstitial melt water		mm
p	Precipitation		mm h^{-1}
T	Temperature		°C
we	Water Equivalent (w.e.)		mm

R2C10: *Page 8, line 18: Please explain and provide examples of these threshold values.*
See R2C2.

R2C11: *Page 9, line9: Given that glaciers cover a very small fraction of the catchment area, could you provide estimates for the remaining 93% of the area?*
See R2C4. Glaciers are included within the bare soil/rocks land use.

R2C12: *Page 10, line 18: I guess this is not the correct symbol.*
Thanks, corrected.

R2C13: *Page 10, line 28: Maybe you could consider reporting the figure as supplementary material or as the new Figure 4, if the current one will be merged with Figure 3.*
We merged Figures 3 and 4 in the revised version (see the following comment R2C14).

R2C14: *Fig 3-4: I think Figure 4 could be merged with Figure 3 in order to have only one figure but with two plots. Please consider this change.*
Done, see the new figure below.

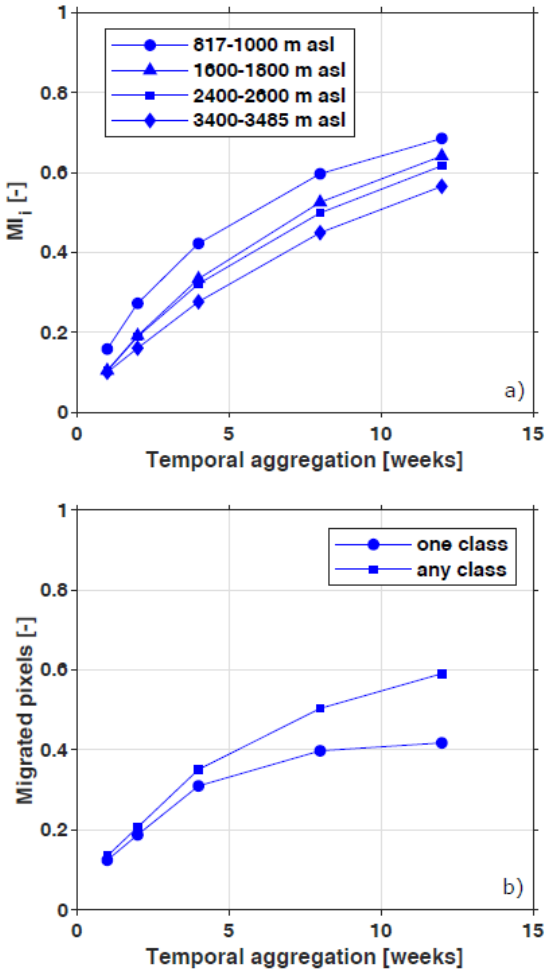

Figure 3. a) Band migration index for the five temporal aggregations, reported for four elevation bands (lowest elevation band from 817 to 1000 m); from 1600 to 1800 m; from 2400 to 2600 m; highest elevation band from 3400 to 3485 m). b) Fraction of migrated pixels computed for the five temporal aggregations over all the elevation bands. Circles refers to pixels that migrated of ±1 energy class, squares to total migrated pixels.

R2C15: *Page 13, line 6: Please provide the fraction for the different land uses in the description of the study area. I think coniferous forests and discontinuous vegetation might be the dominant land covers in such a catchment. Therefore, given the limits of MODIS in vegetated areas, I would suggest to show the comparison between TOPMELT and MODIS for all the land covers, except for the forested areas. As an alternative, the results of the comparison could be shown in a table or in the figures, but distinguishing the various land covers.*
See R2C3 and R2C4. In the revised version, we added text with the fraction of different land use cover.

R2C16: Figure 5: Please report also in the caption of the figure what TP, TN, FP and FN represent.
Done.

R2C17: line2 Page 14: Please revise the English because the second part of the sentence is not clear.
Done

R2C18: *Fig 8: Please use the same scale for NSE and add a) and b) in the two plots and the caption of the figure.*

Done, see below revised Figure 7.

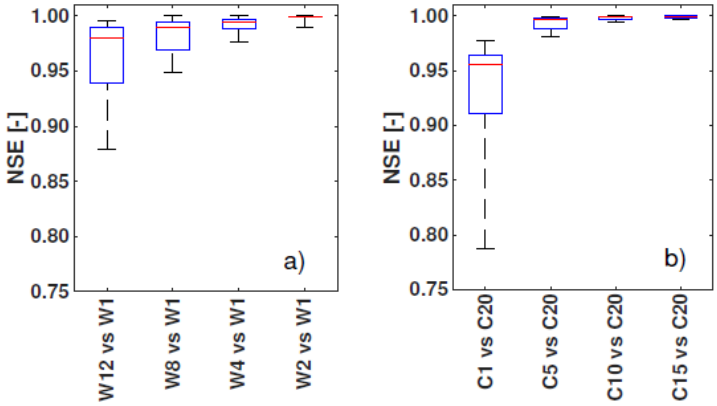

Figure 7. Box plots of NSE computed from the pixel by pixel comparison of the a) temporal and b) spatial aggregation series of SWE maps, from October 2010 to June 30 2011 at weekly time-step. On each box, the central mark indicates the median, and the bottom and top edges of the box indicate the 25th and 75th percentiles, respectively. The whiskers extend to the maximum and the minimum efficiency. The reference is TOPMELT with W1-C10 configuration for the plot of the left panel, W4-C20 for the plot on the right.

R2C19: *Page 15, line 11: Why should W4-C10 be the better choice considering accuracy and computational efficiency? Based on Figure 8, I would choose W2-C10. Please explain the sentence (your choice) and especially from the computational efficiency point of view.*
For this case study, results obtained with the finest spatial and temporal aggregation are similar to those obtained with an intermediate configuration (W4-C10), despite W2-C10 performs better. TOPMELT, in its W4-C10 configuration, computes the snowpack model for 10 points (classes) and updates the radiation 12 times a year; on the other hand, the W1-C20 configuration performs double the load for computing the snowpack (20 classes) and updates the radiation distribution four times more (48 times a year). Therefore, an intermediate resolution represents a balance between computational efficiency and accuracy. We added this to the revised paper.

Reviewer 3 Anonymous

Main Comments

R3C1: The structure could be improved. 1) in the Introduction, the manuscript should emphasize the gap and importance of the research and how you are going to achieve, instead of model introduction as in lines 21-35 (page 2) and lines 1-10 (page 3).2) Section 4 kind of mixes the methodology and model results.

In the revised version, we improved the Introduction by pointing out three important implications of integrating ETI snowpack models into semi-distributed runoff models. 'Integration of ETI snowpack models into lumped or semi-distributed hydrological models may have the potential to increase spatial transferability of calibrated snowpack model parameters for hydrological applications over ungauged mountainous basins, as shown by Comola et al. (2015). Another important implication of the stronger physical basis of the ETI model with respect to simpler 'degree day' models is that it might be more appropriate for the study of climate-change impact on melt regimes, as shown by Pellicciotti et al. (2005). Finally, increasing the accuracy of the modelled snow

water equivalent may improve the outcomes of data assimilation procedures of remotely sensed snow cover information.'

We substantially modified Section 4 by including analyses of scale dependency of radiation aggregation level. For this, we examined the control exerted by the catchment size on runoff simulations. We subdivided the study basin into a number of sub-basins characterised by different drainage areas. We isolated 5 basins with mean drainage of 20 km^2, 10 basins with mean drainage area of 10 km^2, and 20 basins with mean drainage area of 5 km^2. Results are reported in the new Section 3.4 of the revised version (also, see the answer to the next comment).

R3C2: The model calibration is too short. For new model introduction, people are interested in model parameters, their sensitivities, or how to estimate these parameters. It is not clear here.

The revised Sections 4.3 and 4.4 have been substantially modified, by including new work on the model sensitivity to spatial and temporal aggregation levels. We added a table (see Table 2 below) reporting the results of the validation for different model aggregation in space and time. It is evident from results that the model is not sensitive to different configurations: this is due to the relatively large size of the basin. This basin size was chosen not to get best model performance, but to demonstrate model functionality in terms of output products and possible applications.

As aforementioned in the answer to comment R3C1, we also examined the influence of the catchment size on runoff simulations. We subdivided the study basin into a number of sub-basins with different drainage areas. We isolated 5 basins with mean drainage of 20 km^2, 10 basins with mean drainage area of 10 km^2, and 20 basins with mean drainage area of 5 km^2. Results are reported in the new Section 4.4 of the revised paper. We added an additional table (Table 3, reported below) showing the sensitivity of the TOPMELT-ICHYMOD model to the catchment size .

Table 2. Validation performance of the TOPMELT-ICHYMOD model at different spatial aggregation and temporal resolution, from October 2001 to October 2007.

W4C1	**W4C5**	**W4C10**	**W4C15**	**W4C20**
0.73	0.73	0.71	0.73	0.73
W1C10	**W2C10**	**W4C10**	**W8C10**	**W12C10**
0.71	0.71	0.71	0.70	0.71

Table 3. Mean value of the Nash-Sutcliffe index (NSE) of the comparison between W4C1 and W4C10 TOPMELT-ICHYMOD simulated flows and the reference flow simulations, obtained by using the W4C20 set up, over basins of three different drainage areas: 5, 10 and 20 km^2. Comparisons carried out over the March. 1 to June, 30 period.

Model set-up	**Sub-basin area**		
	5 km^2	10 km^2	20 km^2
W4C1	0.77	0.91	00.99
W4C10	0.97	0.99	0.99

R3C3: Comparison results are also missing. For example, there is only one simulation presented in Figure 6, while there are so many simulations have been done (if I am right). How does snow parameters affect hydrograph or snow cover? (see also point 2 above).

See our response to comment R3C2.

R3C4: I am not clear how radiation is calculated. Is it based on station data or theoretical solar radiation equation? How did MODIS data come into play? Section 2.1 and/or section 4.1 could explain something on this.

Radiation is computed theoretically based on the models mentioned in Section 2.1 'Clear sky potential radiation computation and derivation of radiation distribution'.

R3C5: The integration of TOPMELT and ICHYMOD is also not clear, especially on the routing. My understanding is that ICHYMOD is a lumped model and its routing scheme shouldn't consider elevation bands. Then how is water from each cell (combination of elevation bands and radiation classes) routed to the outlet?

ICHYMOD is a semi-distributed model which spatially aggregates the TOPMELT water output generated by the combination of elevation bands and radiation classes to provide a lumped input to the model soil module (which accounts for infiltration and groundwater storage). Hence, the routing scheme is a lumped description of the water transfer at the basin scale, through both slow and fast pathways. We modified the text in the presentation of ICHYMOD to highlight this feature.
.

R3C6: English is readable. However a native speaker might improve the manuscript

Thanks, the work was checked by a native English speaker.

R3C7: Section 5 seems more like a summary
We modified the conclusions to highlight the implications of the results obtained in this work

Minor comments

R3C8: Line 24 of page 1 and Line 1 of page 2. I don't understand the logic

We are here introducing two extreme modelling approaches: the temperature index based modelling (simplified but efficient) and physical modelling (more realistic but complex). We do this to introduce TOPMELT approach, which is intermediate.

R3C9: There is a duplication (line 29 of page 3, and line 1 of page 4)

Corrected

R3C10: Equation 1.What is the range of G

The range of G is limited to positive values. Since the precipitation gradient is linear with the elevation with slope governed by G, the precipitation can become negative at lower elevation bands for increasing values of G. In this case the code automatically limits the gradient, providing an automatic correction.

R3C11: Figure 6: add the content of bottom plot in the caption.

Content added.

R3C12: Figure 7: why don't you use the whole simulation period?

We do not show the whole simulation period because we wanted to focus on an active snow melting phase. We chose this period in particular because the sample MODIS map of Figure 7 falls within this time range.

R3C13: 'reference fields' in the second last line of Page 14: what are they?

We changed 'fields' to 'SWE distribution over space'. We better explained what we meant by 'reference' for Figure 8, both in the text and the caption.

R3C14: Figure 8: What is your point? To me, models with similar spatial or temporal resolution should give similar results.

We wanted to yield In Figure 8 the sensitivity of modelled SWE spatial distribution to different model configurations. To do so, the finest temporal and spatial model configuration was chosen as reference or Figure 8a and Figure 8b respectively. Additionally, please see our response to comment R1C4.

REFERENCES

Anderson, E.A.: A Point Energy and Mass Balance Model of a Snow Cover. Silver Spring, Md.: U.S. Dept. of Commerce, National Oceanic and Atmospheric Administration, National Weather Service, Office of Hydrology, 1976.

Borga M. and Vizzaccaro A.: On the interpolation of hydrologic variables: formal equivalence of multiquadratic surface fitting and kriging, J. Hydrol., vol. 195, no. 1–4, pp. 160–171, doi:10.1016/S0022-1694(96)03250-7, 1997.

Comola, F., B. Schaefli, P. Da Ronco, G. Botter, M. Bavay, A. Rinaldo, and M. Lehning: Scale-dependent effects of solar radiation patterns on the snow-dominated hydrologic response, Geophys. Res. Lett., 42, 3895–3902, doi:10.1002/2015, 2015.

Parajka, J., and Blöschl, G.: Spatio-temporal combination of MODIS images - potential for snow cover mapping, Water Resour. Res., 44, W03406, doi:10.1029/2007WR006204, 2008.

Pellicciotti, F., Brock, B., Strasser, U., Burlando, P., Funk, M. and Corripio, J.: An enhanced temperature-index glacier melt model including the shortwave radiation balance: development and testing for Haut Glacier d'Arolla, Switzerland, J. Glaciol., 51(175), 573–587, doi:10.3189/172756505781829124, 2005.

TOPMELT 1.0: A topography-based distribution function approach to snowmelt simulation for hydrological modelling at basin scale

Mattia Zaramella[1], Marco Borga[1], Davide Zoccatelli[1], and Luca Carturan[1,2]

[1]Department of Land, Environment, Agriculture and Forestry, University of Padua, Padova, 35020, Italy
[2]Department of Geosciences, University of Padua, Padova, 35131, Italy

Correspondence: Mattia Zaramella (mattia.zaramella@unipd.it)

Abstract. Enhanced temperature-index distributed models for snowpack simulation, incorporating air temperature and a term for clear sky potential solar radiation, are increasingly used to simulate the spatial variability of the snow water equivalent. This paper presents a new snowpack model (termed TOPMELT) which integrates an enhanced temperature index model into ~~a lumped~~ th ICHYMOD semi-distributed basin scale hydrological model by exploiting a statistical representation of the distribution of clear sky potential solar radiation. This is obtained by discretising the full spatial distribution of clear sky potential solar radiation into a number of radiation classes. The computation required to generate a spatially distributed water equivalent reduces to a single calculation for each radiation class. This turn into a potentially significant advantage when parameter sensitivity and uncertainty estimation procedures are carried out. The ~~model includes a routine, which accounts for the variability of clear sky radiation distributions with time , ensuring a consistent temporal simulation of the snow mass balance~~radiation index may be also averaged in time over given time periods. Thus, the model resembles a classical temperature-index model when only one radiation class for each elevation band and a temporal aggregation of one year is used, whereas it approximates a fully distributed model with increasing the number of the radiation classes ~~(and correspondingly decreasing the area corresponding to each class)~~and decreasing the temporal aggregation. TOPMELT is ~~applied~~ integrated within the semi-distributed runoff model and it is applied at hourly time step over the Aurino basin at S. Giorgio, a 614 km^2 catchment in the Upper Adige river basin (Eastern Alps, Italy) to examine the sensitivity of the snowpack and runoff model results to the ~~temporal and spatial aggregation of the radiation fluxes.~~ spatial and temporal aggregation of the radiation fluxes. It is shown that the spatial simulation of the snow water equivalent is strongly affected by the aggregation scales. However, limited degradation of the snow simulations is achieved when using ten radiation classes and four weeks as spatial and temporal aggregation scales, respectively. Results highlight that the effects of space-time aggregation of the solar radiation patterns on the runoff response are scale dependent. They are minimal at the scale of the whole Aurino basin, while considerable impact is seen at a basin scale of 5 km^2.

1 Introduction

Seasonal snow cover is an important storage and source of melt water for human use, irrigation and hydropower production in many regions of the world. On the other hand, snow cover and melt water can be a cause of disastrous natural hazards, such as floods and avalanches. Additionally, snow cover is a key factor in the weather and climate system, both regionally and

globally (Armstrong et al. , 2008). Owing to the society's strong need for updated information on snow conditions, snow accumulation and melt, models have been developed with a wide range of features. Approaches for snowpack computation range from empirical models (e.g. simple temperature index models) to more-sophisticated physically based energy-balance models ~~(Avanzi et al. , 2016; Magnusson et al., 2015; Essery et al., 2013; Vionnet et al., 2012)~~(Zappa et al., 2003; Vionnet et al., 2012; Essery et a
. Temperature-index models require only temperature as input and are based on the assumption of a linear relationship between this variable and melt rates, whereas energy-balance models are based on the computation of all relevant energy fluxes at the snowpack surface, and thus require extrapolation of numerous meteorological and surface input variables at local scale (Jóhannesson et al., 1995; Cazorzi and Dalla Fontana, 1996; Hock, 1999; Hock and Holmgren, 2005; Anslow et al. , 2008; Formetta et al., 2014). Advances over the simple dependence of melt on air temperature by addition of radiation terms have been suggested in the last decades ~~(e.g. Hock, 1999; Pellicciotti et al., 2005, Carturan et al., 2012),~~ (Hock, 1999; Pellicciotti et al., 2005; Carturan et al., 2012), and are termed enhanced temperature-index models (ETI) here. In contrast to simple temperature-index models, where melt varies in space only as a function of elevation (given by temperature lapse rates), ETI models includes a term for clear sky potential solar radiation. This term accounts for topographic effects (e.g. aspect, slope and shading) on the spatial distribution of melt, without the need for additional meteorological variables (e.g. global radiation and cloud data). ETI models have been found to provide a better representation of the spatial and temporal variability of melt controlled by solar radiation, when compared with simple temperature index models, as reported by a number of authors (Cazorzi and Dalla Fontana, 1996; Hock, 1999; Pellicciotti et al., 2005; Carenzo et al., 2009 among others). Some of these approaches also better cope with the physical character of the melt process and provide a promising approach to modelling the snowpack at the catchment scale with fewer input data than energy-balance models, but allowing better model parameter transferability than standard temperature-index models (Carenzo et al., 2009).

In spite of their improved accuracy compared to simpler approaches, ETI models have been so far not integrated within lumped or semi-distributed, basin-scale hydrological modelling schemes, which are still frequently used to model sparsely gauged mountainous catchments. Integration of ETI snowpack models into lumped or semi-distributed hydrological models may have the potential to increase spatial transferability of calibrated snowpack model parameters for hydrological applications over ungauged mountainous basins, as shown by Comola et al. (2015). Another important implication of the stronger physical basis of the ETI model with respect to simpler 'degree day' models is that it might be more appropriate for the study of climate-change impact on melt regimes, as shown by Pellicciotti et al. (2005). Finally, increasing the accuracy of the modelled snow water equivalent may improve the outcomes of data assimilation procedures of remotely sensed snow cover information. In a few cases, ~~lumped models have been proposed which incorporate~~ semi-distributed models incorporating a spatial discretization in classes of elevation and aspect ~~classes~~ have been applied to represent the effect of ~~different expositions~~ exposition on snow melt and ~~adjusting accordingly the model snowpack parameter (Konz and Seibert, 2010; Abudu et al. , 2016)~~adjust snowpack parameters accordingly (Klok et al., 2001; Konz and Seibert, 2010; Abudu et al. , 2016). In other cases, a mean value of radiation has been used over the basin area in the same elevation band, modifying accordingly the melt parameters (Li and Williams, 2008). However, these types of tessellation have no allowance for representing the actual variations of radiation distribution over space and time, which is an important feature in ETI models (Pellicciotti et al., 2005).

This work describes a novel snowpack model (termed TOPMELT herewith), which integrates the ETI snowpack method originally developed in a spatially distributed way by Cazorzi and Dalla Fontana (1996) within a ~~lumped~~ semi-distributed basin-scale hydrological model. In the model developed by Cazorzi and Dalla Fontana (1996), local snowmelt is computed by using a combined melt factor which is multiplied by a radiation index and positive air temperature. With TOPMELT, pixels with similar radiation index and air temperature are identified by subdividing basin elevation bands into a number of radiation index classes. Then, the snowpack modelling is carried out for each class of radiation index and for each elevation band. This ensures to achieve the significant computational efficiency, which characterizes the temperature index models, allowing at the same time the ~~higher accuracy~~ stronger physical basis of ETI models. This is a potentially significant advantage when several model simulation runs should be carried out, such as in Monte Carlo based parameter sensitivity and uncertainty estimation procedures~~are carried out~~.

The model accounts for the temporal variability of the radiation index by using local mean values of the index computed over given temporal aggregation intervals, ranging from one to several weeks . This means that a time-averaged solar radiation distribution is used over a given temporal interval, before substituting it with a new averaged distribution. With decreasing the updating interval, the accuracy of the model is expected to increase at the expenses of the computational efficiency.

As the spatial distribution of clear sky solar radiation changes with time, a radiation class computed ~~at two different times corresponds to two different areas~~ over two different periods may sample two different portions of the elevation band. This means that a pixel belonging to a certain class at a given time, will belong to a different class at another time. TOPMELT incorporates a time-integration routine, which accounts for the temporal variability of the radiation index distribution, ensuring a consistent temporal simulation of the snowpack. Thus, TOPMELT permits full implementation of the ETI snowpack method taking into account the seasonal evolution of the spatial distribution of solar radiation. Moreover, it provides a spatially continuous mapping of simulated snow water equivalent, in spite of the computationally-efficient ~~lumped~~ semi-distributed representation of basin-scale snowpack modelling. Depending on the number of radiation classes which are used in the model, the snowpack model makes use of solar radiation values which are spatially averaged over different areas. Effectively, the model resembles a classical temperature-index model when only one radiation class for each elevation band is used, whereas it approximates a fully distributed model with increasing the number of the radiation classes (and correspondingly decreasing the area corresponding to each class).

~~The balance between computational efficiency and model accuracy is not only affected by the spatial averaging of the radiation values. The model permits also the use of temporally averaged values of solar radiation values. This means that a time-averaged solar radiation distribution is used over a given temporal interval (termed here updating interval), before substituting it with a new averaged distribution. With decreasing the updating interval, the accuracy of the model increases at the expenses of the computational efficiency.~~

This paper describes in detail the structure of TOPMELT and of the time-integration routine. The integration of TOPMELT within the ICHYMOD hydrological model is also illustrated. Finally, results are reported from the application of TOPMELT over the 614 km^2 Aurino basin at S. Giorgio in the Upper Adige river system (Eastern Italian Alps). The case study is exploited to i) examine the sensitivity of the snowpack and runoff model results to the temporal and spatial aggregation of the radiation

fluxes, and ii) to identify suitable spatial and temporal aggregation intervals for model simulation. The sensitivity analysis is performed on modelled snowpack in terms of snow water equivalent and on ensueing simulated runoff, comparing the output from simulations performed at different aggregation intervals with a reference represented by the finest aggregation levels.

2 TOPMELT structure

In TOPMELT, the basin area is subdivided into elevation bands to account for air temperature variability with elevation. Then, each elevation band is subdivided into a number of radiation classes. This is carried out by dividing each elevation band into a number n_c of equally distributed radiation classes, where the *i-th* class contains the band sub-area corresponding to the *i-th* percentile of the incident radiation energy. Therefore, the model spatial domain is represented by n_b elevation bands and by n_c radiation classes for each elevation band. ~~Each~~ TOPMELT deals with separate snow and glacier melt: to account for the presence of a glacier area associated to an energy class, one of the $n_b \times n_c$ model cells is ~~characterised by a~~ characterized by the corresponding fraction of glacier area~~and of debris-covered glacier area~~. The spatial subdivisions controls the balance between computational efficiency and model accuracy in the snowpack model.

The following sections describe the main input and modules of the model, where an hourly temporal interval is used for model computations.

2.1 Clear sky potential radiation computation and derivation of radiation distributions

~~Clear~~ For the application of TOPMELT presented in this work, clear sky short wave solar radiation [Wm^{-2}] is computed at each element of the Digital Terrain Model (DTM) by taking into account shadow and complex topography~~. The model estimates~~ , calculating the apparent sun motion (Swift , 1976; Lee, 1978; Oke, 1992) and ~~computes~~ the intersection of radiation with topography (Dubayah et al., 1990; Ranzi and Rosso, 1991). Diffuse radiation is computed by accounting for self-shading (by slope and aspect) and occlusions produced by the visible horizon. ~~Clear sky solar radiation is computed at each DTM grid at any time instant.~~ Since the model uses radiation values averaged over a given time interval, maps of potential radiation averaged over time are also computed. The spatial distribution of time-averaged clear sky solar radiation are ~~computed~~ calculated over each elevation band, and n_c equally distributed radiation classes are identified. For each radiation class, the mean daily cumulated clear sky radiation value is computed (termed Radiation Index RI herewith, [$MJ\ m^{-2}$]) and used in the snowmelt computation. Radiation is pre-processed and provided as model input. Therefore, the relative module is not included in TOPMELT code, but made available as a stand-alone tool (see the code availability section at the end of the paper).

2.2 Computation of precipitation amount and phase

Snow accumulation is computed starting from ~~the estimation~~ estimates of precipitation and air temperature~~over each elevation band. Air~~ , based on air temperature and precipitation data ~~are acquired at hourly time interval~~ from the available weather stations. ~~A single temperature lapse rate is estimated based on temperature data.~~ Similarly to radiation, the model permits use of several techniques, ranging from Thiessen's polygons to multi-quadratic (Borga and Vizzaccaro, 1997) for the estimation of

basin mean areal precipitation values, which are provided to the model as input data. For the analyses reported in this work, the Thiessen method was used to calculate the mean precipitation over the basin. Air temperature data are used to estimate an unique hourly vertical lapse rate for the whole basin.

To account for ~~gage~~ gauge catch deficiencies that occur during periods of snow, precipitation data are corrected with a Snow Correction Factor (~~SCF~~SCF). This is a multiplier of the precipitation data which is applied when station temperature is lower than a threshold temperature T_c.

~~Mean basin areal precipitation values are obtained by using techniques ranging from Thiessen's polygons to multi-quadratic and Kriging methods.~~ Finally, the basin precipitation value ~~P_{basin}~~ p_{basin} is obtained by applying a non-dimensional Precipitation Correction Factor (~~PCF~~PCF) to account for poor spatial representativeness of rain-gauge stations. ~~The~~

TOPMELT computes the precipitation value at the *i-th* elevation band ~~P_i~~ p_i [mm h^{-1}] ~~is obtained~~ by using a vertical precipitation gradient, accounting for increased precipitation over elevation. Based on results from Tuo et al. (2016), this is obtained by means of a precipitation gradient ~~G~~ G [~~%~~ km^{-1}], as follows:

$$Pp_i = Pp_{basin} \cdot \left(1 + G \cdot \frac{H_i - H_{ref}}{1000} \frac{h_i - h_{ref}}{1000}\right) \quad (1)$$

where ~~H_i and H_{ref}~~ h_i and h_{ref} [m a.s.l.] are the mean altitude of the *i-th* elevation band and of the basin respectively. Eq. 1 is applied in a way to modify only the distribution of precipitation across the elevation bands without altering the value of ~~P_{basin}~~p_{basin}.

~~A~~ PCF and G parameters are generally obtained by comparing model-based snow cover simulations with satellite-based snow-cover estimates. Since the average areal precipitation p_{basin} is a TOPMELT input, only G is a TOPMELT parameter. Optionally, TOPMELT permits to provide a different precipitation value precipitation for each elevation band.

Temperature T_i [°C] is provided as input for each elevation band and time step. In this work, a mean value of air temperature T_i over the *i-th* elevation band is obtained by using the aforementioned vertical temperature lapse rate. Estimation of precipitation phase (solid or liquid) is therefore performed over each elevation band, according to the ~~temperature lapse rate and the~~ threshold temperature T_c.

2.3 Computation of snow and ice melt

For the generic model cell represented by the *i-th* elevation band and the *j-th* radiation class, snow melt rate ~~$F_{i,j}(t)$~~ $f_{i,j}(t)$ [mm h^{-1}] at time t, is computed taking into account air temperature, clear sky radiation and albedo. During day hours, the snowmelt is given by:

$$Ff_{i,j}(t) = CMF \cdot RI_{i,j}(t) \cdot \left(1 - alb1 - ALB_i(t)\right) \cdot \max\left[0, (T_i(t) - T_b)\right] \quad (2)$$

where: $T_i(t)$ is the elevation band temperature, $RI_{i,j}(t)$ [~~J~~MJ m^{-2}h^{-1}] is the cell radiation index, CMF [mm °C^{-1}~~J~~MJ^{-1}m^2] is the combined melt factor, accounting for both thermal and radiative effects; ~~$ALB_i(t)$~~ $alb_i(t)$ [-] is the albedo of snow, $T_b = 0$

°C is a threshold base temperature. Snow albedo is computed for each elevation band based on Brock et al. (2000):

$$ALBalb_i(t) = ALBS - \beta_2 \cdot \left[\log_{10} \sum_k T_i(t_k)\right] \quad (3)$$

where $ALBS$ [-] is the fresh snow albedo, β_2 [-] is a dimensionless parameter, $\sum_k T_i(t_k)$ [°C] is the sum of the positive hourly temperatures exceeding the threshold base temperature T_b since the last snowfall until the current time t.

During night hours, snow melt is simulated ~~by~~ accounting only for air temperature, as follows:

$$Ff_{i,j}(t) = NMF \cdot \max[0, (T_i(t) - T_b)] \quad (4)$$

where NMF [mm h^{-1} °C^{-1}] is the ~~night melt factor~~Night Melt Factor.

For rain-on-snow conditions (Anderson , 1976), melting is computed depending on air temperature and on the energy provided by rain:

$$Ff_{i,j}(t) = \left[RMF + \frac{P_{i,j}(t)}{cost} \frac{p_{i,j}(t)}{COST}\right] \cdot \max[0, (T_i(t) - T_b)] \quad (5)$$

where RMF [mm h^{-1} °C^{-1}] is the ~~rain melt factor and cost~~ Rain Melt Factor and $COST$ [°C^{-1}] is a parameter accounting for the influence of rain on snowmelt (Carturan et al., 2012). For each model cell, the snow water equivalent (~~$WE_{i,j}$~~ $we_{i,j}$ [mm]) is updated by accounting for snow accumulation, rain-on-snow, melt and freezing water. Water due to snowmelt or rainfall is first retained in the snowpack as interstitial water termed ~~Liquid Water $LIQW_{i,j}$~~ liquid water $liqw_{i,j}$ [mm]. When Liquid Water exceeds a water holding capacity of the snowpack (termed LWT), this propagates through the snowpack at a rate $DYTIME$ [m h^{-1}], to form net water flow at the snowpack base.

When air temperature is less than the threshold base temperature, part of the liquid water refreezes and ~~$LIQW_{i,j}$~~ $liqw_{i,j}$ is reduced and added to the snowpack through a freezing rate, termed ~~ICE~~ ice [mm h^{-1}]. This is computed as:

$$ICEice_i(t) = REFRZ \cdot \min[0, (T_b - T_i(t))] \quad (6)$$

where T_b is the threshold base temperature (Eq. 2) and $REFRZ$ [mm °C^{-1} h^{-1}] is the freezing factor. When ~~$WE_{i,j}$~~ $we_{i,j}$ is less than a threshold (termed $WETH$), ice melt starts. This is computed similarly to snow (Eq. 2), but where the snow albedo is replaced by a constant glacial albedo, $ALBG$ [-], as follows:

$$Ff_{i,j}(t) = CMF \cdot RI_{i,j} \cdot (1 - ALBG) \cdot \max[0, (T_i(t) - T_b)] \quad (7)$$

~~In case of debris cover, ice melt is reduced accordingly with the following relationship (Östrem, 1959):~~

$$F_{i,)}(t) = CMF \cdot RI_{i,j} \cdot (1 - ALBG) \cdot T_i(t) \cdot \left[1 - \frac{A^d_{i,j}}{A^g_{i,j}} \cdot \left(1 - e^{-\Gamma}\right)\right] \cdot \max[0, (T_i(t) - T_b)]$$

~~where Γ is a non-dimensional parameter accounting for the geometry of the debris cover (thickness and mean slope); $A^d_{i,j}$ is the debris-covered surface of the glacial area $A^g_{i,j}$ relative to the *j-th* radiation class and *i-th* elevation band.~~ During rainfalls or night hours, glacier melt is computed by means of Eq. 4 and Eq. 5 respectively.

All model parameters and their values are listed in table 1, along with variable names and units.

Table 1. Model parameters and variables: short name, description and measuring units. Parameters are written with capital letters, variables in lowercase.

Parameter	Description	Value	Units
$ALBG$	Glacier albedo	0.3	-
$ALBS$	Fresh snow albedo	0.9	-
β_2	Dimensionless parameter for alb computation	0.0919	-
CMF	Combined Melt Factor	0.013	mm °C^{-1}MJ^{-1}m^2
$DYTIME$	Speed of water propagation through snowpack	3	mh^{-1}
G	Precipitation gradient	0	km^{-1}
LWT	Water holding capacity, fraction of w.e.	0.1	-
NMF	Night Melt Factor	0.16	mm °C^{-1}h^{-1}
$REFRZ$	Freezing factor	0.03	mm °C^{-1}h^{-1}
RI	Radiation Index, mean daily energy	$1 \div 42$	MJ m^{-2}h^{-1}
RMF	Rain Melt Factor	0.3	mm °C^{-1}h^{-1}
T_b	Base temperature	0.0	°C
T_c	Snow/rain threshold temperature	1.5	°C
$WETH$	Water equivalent minimum threshold before ice-melt	5	mm
Variable	**Description**		**Units**
alb	Snow albedo (accounting for aging)		-
h	Elevation		m
f	Fusion		mm h^{-1}
ice	Freezed water		mm
$liqw$	Interstitial melt water		mm
p	Precipitation		mm h^{-1}
T	Temperature		°C
we	Water Equivalent (w.e.)		mm

2.4 Updating the Radiation Index distribution: the time-integration routine

As reported in the previous sections, the spatial distribution of clear sky solar radiation changes with time, based both on astronomic variation of the radiation flux and its interaction with a complex topography. This implies that the statistical distribution of the radiation index over each elevation band will be also modified and should be updated. In general ~~,~~ a radiation class, computed at two different ~~times~~ time steps, covers two different areas of the elevation band. ~~This means that~~ Thus, a pixel belonging to a certain class at a given time ~~,~~ will belong to a different class at another time. Figure 1 shows two different maps

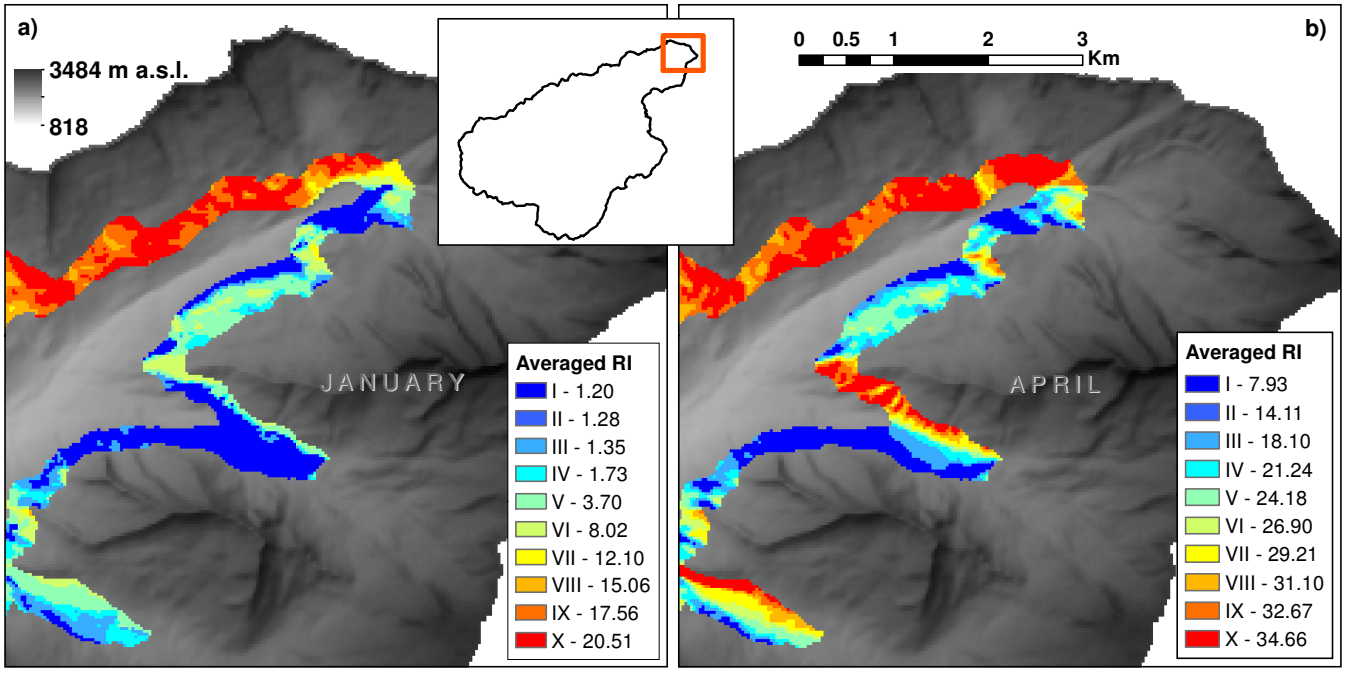

Figure 1. Comparison between radiation index distribution over the 2000-2200 m elevation band of the Aurino basin for a) January 1st and b) April 1st (ten classes subdivision). The figures show the north-eastern portion of the basin and report the average radiation index [J m^{-2} ~~h^{-1}~~], with the corresponding radiation class identified by a roman number.

of ~~RI~~*RI*, (representing January 1 and April 1, from an elevation band ranging from 2000 to 2200 m a.s.l., taken from the basin selected for the case study of this work. The radiation index is distributed using ten equally-distributed classes. While the radiation index varies from 1.2 to 20.5 MJ m^{-2} ~~h^{-1}~~ in January, it ranges from 7.9 and 34.7 MJ m^{-2} ~~h^{-1}~~ in April. However, differences are not restricted to the magnitude of the index. Despite each class has the same area within the elevation band, their spatial distribution changes from one map to the other. Examination of the figures shows that a number of pixel belonging to Class V in January are included in Class IX in April. Since the two snowpack state variables, ~~*WE* and *LIQW*~~ *we*(t) and *liqw*(t), are computed at the model cell level, pixel transition from a given cell to another must be accounted for, whenever the radiation index distribution is updated with time (termed switch date here). To account for pixel transition through classes, TOPMELT implements an adjusting procedure for model state variables. The procedure is here described applied to the arbitrary cell state variable ~~$X_{i,j}$~~ $x_{i,j}$, corresponding to the *i-th* elevation band and the *j-th* radiation class of the basin. When updating from one radiation index map to another, pixels from a certain class can, in principle, move to all other classes, and pixels from other classes can conversely move to that class. The ~~$X_{i,j}$~~ $x_{i,j}$ variable, which corresponds to certain model cell, should be updated accordingly. Therefore, a 2-D array accounting for pixels transition and the associated variables among classes is defined, namely the transition matrix $\mathbf{M}_i$ of the *i-th* elevation band.

The transition matrix is $n_c \times n_c$ sized and is computed for each elevation band and is unique for each switch date of the radiation index maps. The element $M_{i,j,k}$ of the matrix represents the number of pixels moving at a switch date from the *j-th* source class to the *k-th* destination class, within a given elevation band i. $M_{i,j,j}$ is the diagonal element of $\mathbf{M}_i$, representing the pixels that did not move from the source radiation class. Provided that the total number of pixels belonging to a class must remain constant, a property of the transition matrix is that the sum of the elements along the *i-th* row is equal to the sum of the elements of the *j-th* column (i.e. the number of pixels leaving a class is replaced by an equivalent number of pixels migrating from other classes):

$$\sum_{h=1}^{n_c} M_{i,j,h} = \sum_{h=1}^{n_c} M_{i,h,j} = N_{i,j} \tag{8}$$

where $N_{i,j}$ is the number of pixels in the *j-th* radiation class within the *i-th* elevation band. When TOPMELT switches from one radiation index map to another, the cell state variable ~~$X_{i,j}$~~ $\tilde{x}_{i,j}$ in the new model cell will be the sum of the pixel contribution from other classes and of the pixels remaining in the source class, where the number of incoming or remaining pixels is weighted with respect to the total number of pixels of the source class. Therefore, ~~$X_{i,j}$~~ $\tilde{x}_{i,j}$ is corrected through a matrix $\mathbf{C}_i$ of correction coefficients, relative to the *i-th* elevation band, which can be derived from $\mathbf{M}_i$ through the following relation:

$$C_{i,j,k} = \frac{M_{i,j,k}}{N_{i,j}} \tag{9}$$

Follows from Eq. 8 and Eq. 9 that the sum of each line or column of the correction factors matrix $\mathbf{C}_i$ must be equal to 1:

$$\sum_{j=1}^{n_c} C_{i,j,k} = \sum_{j=1}^{n_c} \frac{M_{i,j,k}}{N_{i,j}} = 1 \tag{10}$$

The coefficient $C_{i,j,k}$ represents the correction factor for the state variable ~~$X_{i,j}$~~ $\tilde{x}_{i,j}$ that must be redistributed among the other classes through the updating process, within the *i-th* elevation band. With the updating, if ~~$X_{i,j}$~~ $\tilde{x}_{i,j}$ is the source class variable band and ~~$X_{i,j}$~~ $\tilde{x}_{i,j}$ its transformed (i.e. destination), the class variable correction is computed through the following:

$$\widehat{\mathbf{x}}_i = \mathbf{C}_i \cdot \mathbf{X}\tilde{\mathbf{x}}_i \tag{11}$$

or through the equivalent forms:

$$\begin{bmatrix} \widehat{x}_{i,1} \\ \widehat{x}_{i,2} \\ \vdots \\ \widehat{x}_{i,n_c} \end{bmatrix} = \begin{bmatrix} C_{i,1,1} & C_{i,1,2} & \cdots & C_{i,1,n_c} \\ C_{i,2,1} & C_{i,2,2} & \cdots & C_{i,2,n_c} \\ \vdots & \vdots & \ddots & \vdots \\ C_{i,n_c,1} & C_{i,n_c,2} & \cdots & C_{i,n_c,n_c} \end{bmatrix} \cdot \begin{bmatrix} x_{i,1} \\ x_{i,2} \\ \vdots \\ x_{i,n_c} \end{bmatrix} \tag{12}$$

and

$$\widehat{x}_{i,j} = \sum_{k=1}^{n_c} C_{i,j,k} \tilde{x}_{i,k} \tag{13}$$

Eq. 13 represents the weighted sum of ~~$X_{i,k}$~~ $x_{i,k}$ pixels that moved from the n_c source classes to destination *k-th* class. Since the correction factors matrix $\mathbf{C}_i$ can be computed once for all, the model computational efficiency is preserved.

To exemplify the computational flow and its constraints, the example of the water equivalent ~~WE~~ *we* state variable is reported here. At a given radiation index switch, ~~$WE_{i,j}$~~ $we_{i,j}$, will be transferred within the *i-th* elevation band across different classes transforming into ~~$\widehat{WE}_{i,j}$~~ $\widehat{we}_{i,j}$, for $j = 1, n_c$. The total volume of snow at a given elevation band i of the destination distribution is:

$$\widehat{V}_i^{WEwe} = \sum_{j=1}^{n_c} (\widehat{we}_{i,j} N_{i,j} A_p) \tag{14}$$

where A_p is the pixel size. Combining Eq. 13 and Eq. 14, and provided that the number of pixels is the same for each class of the *i-th* elevation band ($N_{i,j} = N_i$ for $j = 1, n_c$):

$$\widehat{V}_i^{WEwe} = N_i A_p \sum_{j=1}^{n_c} \left[\sum_{k=1}^{n_c} \left(C_{i,j,k} WE we_{i,k} \right) \right] = N_i A_p \sum_{k=1}^{n_c} \left(WE we_{i,k} \sum_{j=1}^{n_c} C_{i,j,k} \right) \tag{15}$$

Eq. 10 plus Eq. 15 yield that the transformed ~~WE~~ w.e. volume is equal to original volume:

$$\widehat{V}_i^{WEwe} = N_i A_p \sum_{k=1}^{n_c} WE we_{i,k} = V_i^{WEwe} \tag{16}$$

Therefore, Eq. 10 is a constraint that holds conservation of ~~WE~~ w.e. through the updating process.

2.5 Representation of the water equivalent distribution and snow cover

The model allows to provide the representation of spatially continuous water equivalent maps (as well as any other model cell variable) at a given time. This is carried out by exploiting a routine which links each model cell to the corresponding topographic elements, accounting for variation of the radiation index maps. Then, the water equivalent maps may be ~~easily~~ converted to snow cover maps by using suitable threshold values. In this work, we used a minimum threshold of 10 mm (Parajka and Blöschl, 2008) for the intercomparison with the MODIS snow cover products.

3 TOPMELT integration into ICHYMOD

TOPMELT is integrated within a ~~lumped hydrological model(ICHYMOD, Norbiato et al., 2009),~~ semi-distributed hydrological model, ICHYMOD, (Norbiato et al., 2008), which transforms net precipitation into runoff at the outlet of the basin. The total flow routed from TOPMELT to ICHYMOD is the areal weighted sum of each single cell flow, which is made by rainwater and excess snowmelt water. The model consists of a soil moisture routine and a flow routing routine. ~~Potential evapotranspiration is estimated by using the Hargreaves method (Hargreaves and Samani, 1982).~~

The soil moisture routine uses a probability distribution to describe the spatial variation of water storage capacity across a basin, accordingly with the Probability Distributed Model (PDM) by ~~Moore (2007). Saturation excess runoff generated~~

over the basin is integrated to give the total direct runoff entering the fast response pathways to the basin outlet, represented Moore (2007). Drainage from the soil enters slow response pathways. The base discharge is routed from groundwater to the catchment outlet through a cubic law storage model. Direct runoff from the proportion of the basin where storage capacity has been exceeded is routed by means of a geomorphology-based distributed unit hydrograph (Da Ros and Borga , 1997), conceptualized by a cascade of two linear reservoirs in series. Runoff from ice melt is transferred to the outlet through two different routes, depending on glacial till imperviousness. Part of the ice meltwater is input to the soil moisture storage, while the remaining fraction flows directly to the outlet as a cascade of two linear reservoirs in series.

Drainage from the soil enters slow response pathways. The base discharge is routed from groundwater to the catchment outlet through a cubic law storage model. Storage Storage-based representations of the fast and slow response pathways yield a spatially lumped representation fast and slow response at the basin outlet which, when summed, gives the total basin flow.

Losses due to evapotranspiration are calculated as a function of potential evapotranspiration and the status of the soil moisture store in the PDM. Potential evapotranspiration is estimated by using the Hargreaves method (Hargreaves and Samani, 1982).

4 TOPMELT: Impact of spatial and temporal aggregation scale

4.1 Study site, available data and model set up

TOPMELT is applied in to the Aurino river basin closed at San Giorgio, located in the Adige river system in the Easer Alps, Italy (Figure 2). The basin has an extension of 614 km^2, 2.7% of which covered by glaciers for a total of 16.4 km^2. Forest covers 33.5% of the basin, pasture and grassland 44.5%, bare soil and rocks 21.6% and urban area the remaining 0.4%. Elevation ranges from 817 to 3485 m a.s.l.. Mean annual basin averaged precipitation is around 950 mm, with values ranging from 850 mm at lower elevations to 1300 mm at the highest elevations. Precipitation and temperature data at hourly time intervals are provided by 15 gauging stations (see Figure 2 for locations), whereas observed discharge are available at the stream-gauge station in S. Giorgio Aurino. The natural runoff regime is partially altered by the reservoir operations over the 25 km^2 Neves basin. Basin topography is described by means of a DTM with a 30 m grid resolution.

Satellite observations of snow cover at 250 m resolution are available for the study basin since January 2011 and are provided by an algorithm based on MODIS observations developed by Notarnicola et al. (2013a and 2013b). With this algorithm, MODIS maps provide for each pixel the presence or absence of snow, the presence of clouds, water bodies or pixels with no feature detected. 50 MODIS maps are available during the period from January 1 to June 30, 2011 with a percentage of cloud cover less than 10%.

The basin was subdivided into 14 elevation bands of 200 m each, ranging from 800 to 3600 m above sea level. Elevations bands were then subdivided in a number n_c of radiation classes. To assess the impact of different spatial aggregation levels of the radiation index on model results, five types of class subdivisions of the basin were considered. The elevation bands were divided into n_c=1, 5, 10, 15 and 20 classes, yielding five different spatial aggregation labelled with C1, C5, C10, C15 and C20 respectively. Similarly, to analyse the influence of using different temporal aggregation aggragation periods of the radiation index, five different updating times were used for the computation of the radiation index distribution, with duration

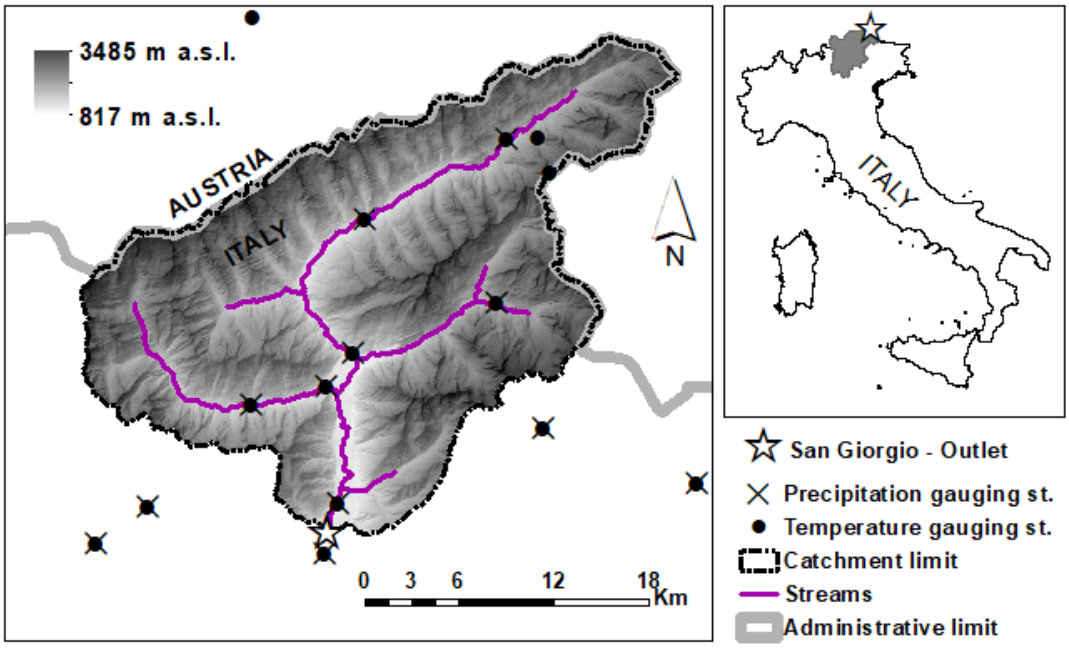

Figure 2. The Aurino river basin closed at S. Giorgio with the position of the hydro-meteorological monitoring stations.

of 1, 2, 4, 8 and 12 weeks and labelled W1, W2, W4, W8 and W12 respectively. Variable temporal and spatial discretization allows for different ~~combinations~~ configurations of the space-time aggregation ~~: for~~ of the radiation index. For example, label W4-C10 refers to a model set up with a temporal aggregation interval of 4 weeks combined with use of 10 radiation classes per elevation band. It is interesting to observe that the model set up W12-C1 resembles a traditional temperature-index model with a radiation correction for elevation band (as in Li and Williams, 2008), whereas the model set-up W1-C20 approximates a fully spatially distributed implementation of the enhanced temperature index model. One should bear in mind that when just one radiation class is used, there is no need to update the distribution of the snow water equivalent.

4.2 The time integration routine: assessment of pixel transition

An important feature of the model is the use of the time-integration routine to ensure consistency in the snowpack simulation. This routine accounts for pixel transition from one radiation index class to another at the switching time. In this section we analyse the pixel transition, by using an index which represents the percentage of migrating pixels over the total number of pixels belonging to a given elevation band, as follows:

$$MI_i = \frac{\widehat{N}_i}{N_i} \tag{17}$$

where MI_i is the migration index of the transition, ~~N_i~~ $\widehat{N_i}$ is the number of pixels changing class during a switch, and N_i is the number of pixels of the *i-th* elevation band.

The percentage of migrating pixels was computed at four elevation bands: the lowest, from the lowest elevation of the basin, 817 m, to 1000 m; two intermediate bands, from 1600 to 1800 m and from 2400 to 2600 m; the highest, from 3400 to 3485 m (which is the max elevation in the basin). The analysis was performed for the five temporal aggregation by using ten radiation index classes, reporting the mean average migration index over the various switches. Results are reported in Figure ~~??~~3a, showing that the percentage of migrating pixels ranges from up to 16% at W1 temporal aggregation to up to 69% at W12 temporal aggregation, with a considerable increase of the transition percentage with the increase of temporal aggregation. It is interesting to observe that the transition percentage decreases with increasing ~~the~~ elevation of the band, i.e. with decreasing the spatial dispersion of pixels corresponding to a certain class. One should note that the results are dependent on the number of radiation classes which are used: results (non reported here for the sake of brevity) show that the migration index increases with the number of classes.

Finally, a specific analysis aimed to analyse the magnitude of the transition class change. To highlight this aspect, the percentage of pixel which moves by only one class (for example from the second to the third radiation class) was computed and compared to the transition percentage. The percentages were computed and averaged for all the elevation bands. Figure ~~??~~ ~~Fraction of migrated pixels computed for the five temporal aggregations over all the elevation bands. Circles refers to pixels that migrated of ±1 energy class, squares to total migrated pixels.~~ 3b shows this comparison, by considering ten radiation classes, for the five temporal aggregations. For aggregation W12, 42% of the pixels migrates through one class, 17% through more than one class and only 41% do not migrate at all. For aggregation W1, 12% of the pixels migrates through one class, only 1% through more than one class and 87% of the pixels do not move from the source class at the switch time. These results agree with those reported in Figure ~~??~~ 3a and underline the impact of using larger temporal aggregations on the pixel transition between various classes.

4.3 Model calibration and validation

The results reported in Section 4.2 are obviously independent on the specification of the snowpack model parameters~~; however~~. However, their impact on model results (for instance, on the snow water equivalent spatial distribution) depends on the specification of model parameters.

TOPMELT and ICHYMOD parameters were identified by means of a two-stage procedure, based on comparison of the simulated outflow with the discharge measured at San Giorgio and on comparison of the simulated snow cover with MODIS data, for the period where MODIS data were available. The model set-up W4-C10 was used for the parameter identification. The following statistics were used for comparing simulated and observed discharges:

$$BIAS = \frac{\sum_{t=1}^{N}(Q_{sim,t} - Q_{obs,t})}{\sum_{t=1}^{N} Q_{obs,t}} \tag{18}$$

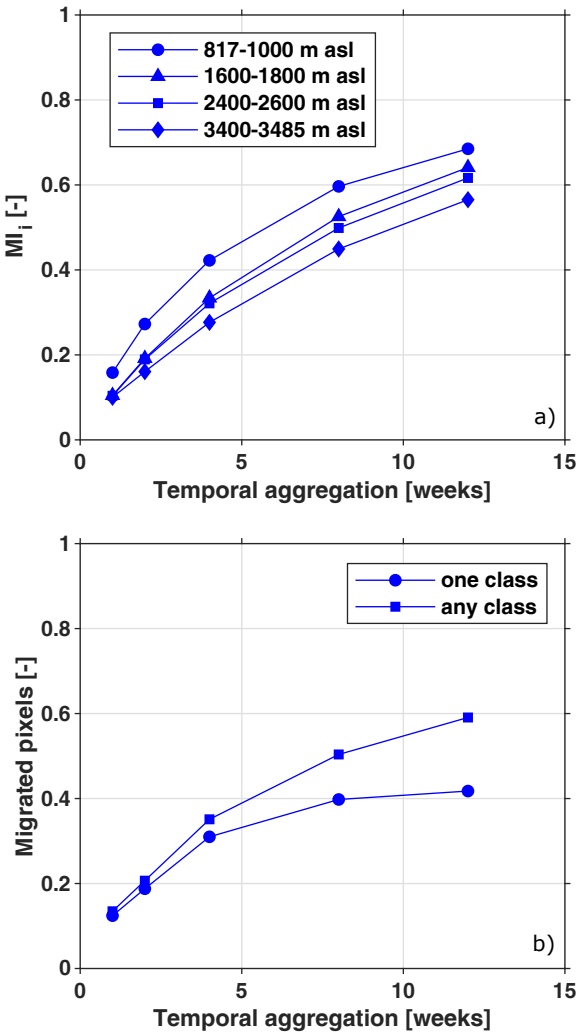

Figure 3. a) Band migration index for the five temporal aggregations, reported for four elevation bands (lowest elevation band from 817 to 1000 m); from 1600 to 1800 m; from 2400 to 2600 m; highest elevation band from 3400 to 3485 m). b) Fraction of migrated pixels computed for the five temporal aggregations over all the elevation bands. Circles refers to pixels that migrated of ±1 energy class, squares to total migrated pixels.

$$NSE = 1 - \frac{\sum_{t=1}^{N} \left(Q_{sim,t} - Q_{obs,t}\right)^2}{\sum_{t=1}^{N} \left(Q_{obs,t} - \bar{Q}_{obs}\right)^2} \tag{19}$$

where $Q_{obs,t}$ and $Q_{sim,t}$ is the observed and simulated discharge at time t, respectively, $\bar{Q}_{obs}$ is the average value of the observed discharges, and N is the number of observations. Optimal values for BIAS and NSE are 0 and 1, respectively.

To compare simulated snow cover (SC) area with MODIS observation, a snow water equivalent threshold of 10 mm was used to declare a snow covered pixel ~~, or conversely a clear one. The threshold was set to 20 mm; it was observed that using lower or higher thresholds within the range 10÷40 mm do not sensibly affect the resulting SC extension.~~ (Parajka and Blöschl, 2008). Then, the ~~30m~~ 30 m grids contributing to one MODIS pixel were calculated, and a simulated MODIS-like pixel was considered as snow covered if the percentage of the snow covered 30 m grid size pixels is equal or higher than 50%. MODIS maps with cloud coverage less than 10% were used for ~~calibration. For analysing~~ the analysis. For assessing the correspondence of simulated versus observed values, the Accuracy Index – ACC skill measure, based on the contingency table, was used:

$$ACC = \frac{TP + TN}{TP + FN + FP + TN} \tag{20}$$

where TP are the number of true positives, i.e. where both model and observation agree on the presence of snow on the pixel; TN is the number of true negatives, FN is the number of false negatives. i.e. pixels which are snow covered according to MODIS and where the model simulates no snow, FP is the number of false positives, i.e. pixels which are free of snow according to MODIS and where the model simulates snow. ACC ranges between 0 and 1 with its optimum at 1. ~~The application of the comparison~~ Application of a comparison between MODIS data and TOPMELT simulated snow cover is exemplified in Figure 4 for a sample date: May 6, 2011. Following Parajka and Blöschl (2008), the Accuracy Index (Eq. 20) was computed on a pixel base over the 50 cloud-free MODIS maps available~~within the calibration period from January 1 to June 30, 2011.~~. The resulting spatial distribution of the Accuracy Index is termed Overall Accuracy (OA) map.

The model parameter identification was carried out by using data from October 1, 2001, to September 30, ~~2012.~~ 2012 by using the model configuration W4-C10. The period from October 1, 2007 to September 30, 2012 was used for model parameter calibration, with ~~optimisation~~ optimization of the statistics BIAS, NSE and ACC~~. The period from~~ , whereas model validation was carried out over the period October 1, 2001, to September 30, ~~2007 was used for model validation. After parameter optimisation,~~ 2007. Model parameter optimization started from the parameterization of the ICHYMOD application by Norbiato et al. (2009). Model error statistics NSE and BIAS ~~values~~ are equal to ~~0,71~~ 0.71 and 2%, respectively, for the calibration period, and to ~~0,72~~ 0.71 and -9%, respectively, for the validation period.

A graphical comparison of simulated (W4C10) and observed discharges is reported in Figure 5 for the period May-July 2011, showing the general consistency of the simulation.

The Overall Accuracy map is reported in Figure 6b, while Figure 6b shows the land use over the catchment. The figure shows that simulated snow dynamics ~~agreed~~ agrees (OA > 0.7) with MODIS snow cover detection by 71% of the area~~(OA > 0.7)~~. Lower OA ~~is due to the~~ corresponds to forest cover, and north facing slope with forest cover are characterised by very low values of OA. This shows clearly the well known combined effect of view geometry and forest cover on MODIS snow cover accuracy. Forests make MODIS remote sensing of snow challenging because the presence of trees complicates monitoring of snow using remote sensing as trees obscure snow on the ground surface ~~(Notarnicola et al., 2013b).~~ (Notarnicola et al., 2013b). View geometry may be a further major error sources in MODIS snow mapping algorithms in forested areas. This is because the gaps in forest canopies, which are essentially the detectable snow fraction in winter, are lower at off-nadir views ~~(Notarnicola et al., 2013b).~~ (Notarnicola et al., 2013b).

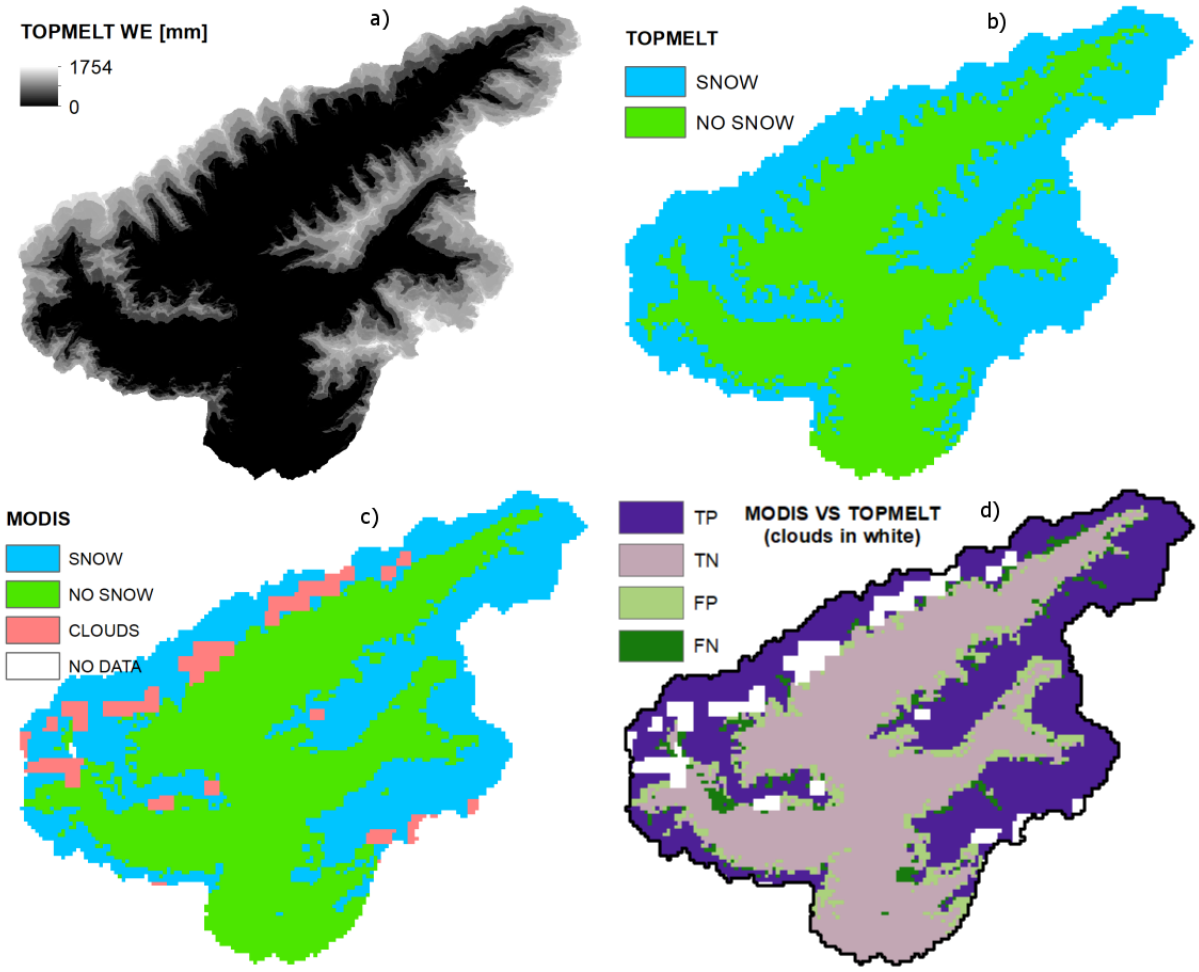

Figure 4. Comparison between simulated and MODIS-derived snow cover map. The comparison is obtained by using the model set up W4-C10 for May 6, 2011. TP nd TN are true positives and true negatives: both TOPMELT and MODIS are indicating the presence or absence of snow at the pixel, respectively. Similarly FP and FN are false positives and false negatives.

4.4 Impact of temporal and spatial aggregation on model results

The impact of using different spatial and temporal aggregation on TOPMELT results was carried out by considering both the spatial distribution of the water equivalent ~~as a key variable~~and the simulated flow. In this analysis, the finest spatial and temporal discretizations, C20 and W1 respectively, were taken as a reference for the the ~~pixel-by-pixel comparisons. The~~ comparisons. For the water equivalent spatial distribution, the assessment was carried out ~~at a weekly time step~~ for the period ~~from~~ between October 1, 2010 ~~to~~ and June 30, 2011~~over 36 maps. This year was selected because MODIS data were available to check the results and the hydrological39 year was an average one.~~, generating a distribution of w.e. at weekly time step, for a total of 50 simulated snow maps. The intermediate subdivision into radiation classes (C10) was used for the comparison of

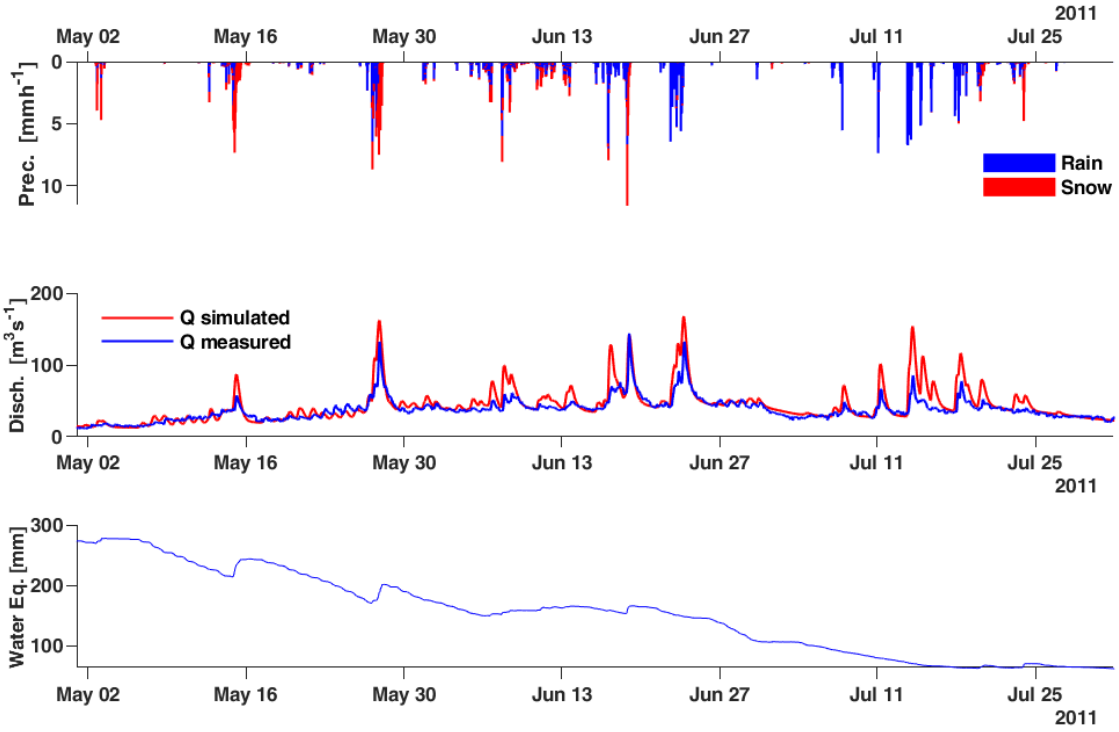

Figure 5. Comparison between simulated (W4-C10) and observed discharge at San Giorgio for the May-July 2011 period. The bottom plot displays the average w.e. over the basin.

temporal aggregations W12 to W2 with W1; on the other hand, the intermediate temporal aggregation of 4 weeks (W4) was used for the comparison of spatial aggregations C1 to C15 with C20 (i.e. the reference configuration for Figure 7a is W1-C10, for Figure 7b is W4C20.

The NSE statistic (Eq. 19) was used to quantify the agreement bewteen the analysis and reference ~~fields~~w.e. distribution over space, by excluding from the comparison all the occurrences of zero water equivalent on both maps. One value of the NSE statistic was obtained for each of the ~~36 maps. The intermediate subdivision into radiation classes (C10) was used for the comparison of temporal aggregations W12 to W2 with W1; on the othe hand, the intermediate temporal aggregation of 4 weeks (W4) ws used for the comparison of spatial aggregations C1 to C15 with C20.~~ 50 maps.

The results are reported in Figure 7, ~~Box plots of NSE computed from the pixel by pixel comparison of the temporal and spatial aggregation series of WE maps, from October 2010 to June 30 2011. On each box, the central mark indicates the median, and the bottom and top edges of the box indicate the 25th and 75th percentiles, respectively. The whiskers extend to the maximum and the minimum efficiency.~~ where the distributions of the NSE statistics are summarised by using box plots. Figure ~~7a~~ 7a summarises the results concerning the impact of the temporal aggregation, whereas Figure ~~7b~~ 7b shows the analysis concerning the spatial aggregation. ~~The impact of using just one radiation class (C1) has a noticeable impact on the results,~~

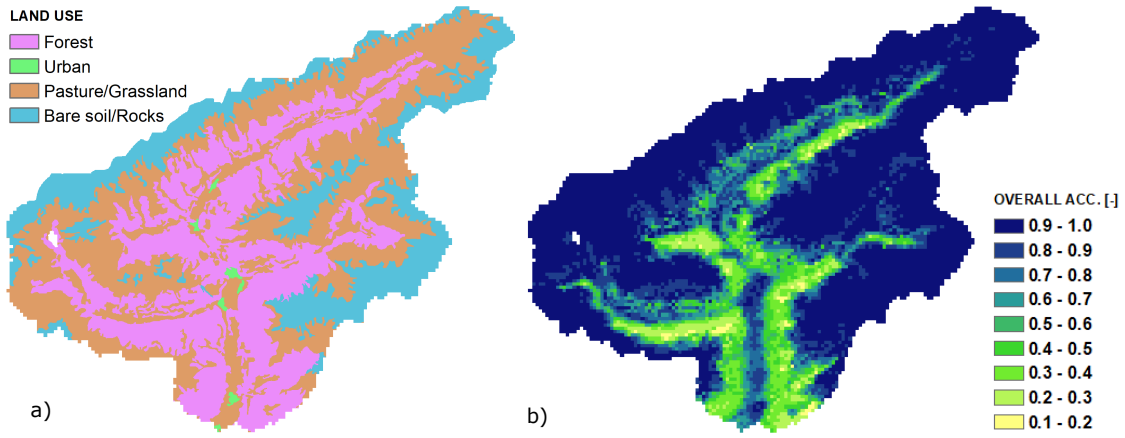

Figure 6. ~~Pixel~~ a) Land use distribution for the catchment and b) pixel based overall accuracy (OA) of the comparison between simulated and MODIS-derived snow cover maps, computed from January 1 to June 30, 2011 for a total of 50 MODIS snow cover maps.

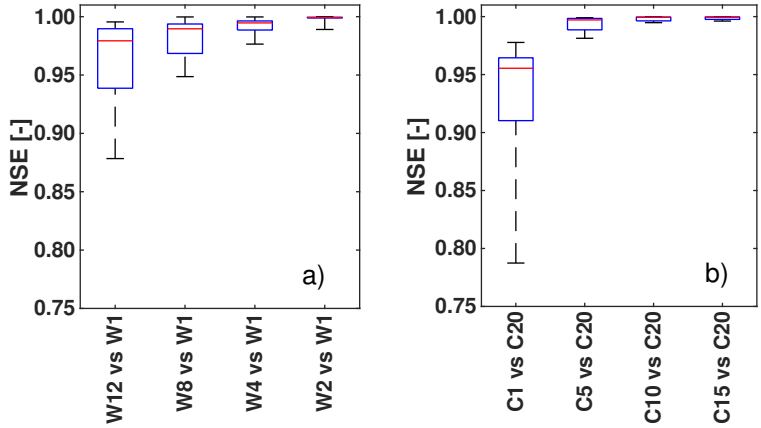

Figure 7. Box plots of NSE computed from the pixel by pixel comparison of the a) temporal and b) spatial aggregation series of w.e. maps, from October 2010 to June 30 2011 at weekly time-step. On each box, the central mark indicates the median, and the bottom and top edges of the box indicate the 25th and 75th percentiles, respectively. The whiskers extend to the maximum and the minimum efficiency. The reference is TOPMELT with W1-C10 configuration for the plot of the left panel, W4-C20 for the plot on the right.

~~with NSE ranging from 0,78 to 0,98. Results improve considerably by using 5 classes (C5). The impact of using the~~ Using the longest temporal aggregation (W12) has ~~less worsening~~ a noticeabe impact on the results, with NSE ranging from ~~0,88 to 0,99.~~ 0.88 to 0.99. Even in this case, a considerable improvement is obtained by using a reduced temporal aggregation, such as ~~W8~~W4. Interestingly, the results resemble the findings obtained by comparing the model set up in terms of pixel migration.

~~The comparison suggests that using the space-time aggregationW4-C10 may provide a good balance between accuracy of the results~~ Using just one radiation class (C1) degrades markedly the accuracy of the WE distribution, with NSE ranging from 0.78 to 0.98. Results improve considerably by using 5 classes (C5).

The impact analysis on flows simulations was carried out by comparing observed and simulated flows over the validation period from October 1, 2001 to September 30, 2007. Results are reported in Table 2 by using the NS efficiency for the various spatial and temporal aggregations. The results are at odd with those reported for the w.e. distribution, showing that the sensitivity of the modelled runoff is negligible. The reported NSE values are very close each other, ranging from 0.70 to 0.73. The comparison of each runoff simulation to the simulations obtained by using the CW reference model, as we did previously for the snow water equivalent maps, results in NSE values always in excess of 0.99. The comparison statistics varied only in a limited way when the comparison was focused on the March. 1 to June, 30 period, i.e. the melting season.

These results are not unexpected. The size of the basin, which largely exceeds the correlation scale of the radiation index, together with the branching nature of the river network, provides indeed a powerful way in averaging out the heterogeneity of snowmelt processes, as shown by Comola et al. (2015), among others.

To better highlight the control exerted by the catchment size on runoff simulations, we subdivided the study basin into a number of sub-basins characterised by different drainage areas. We isolated 5 basins with mean drainage of 20 km^2, 10 basins with mean drainage area of 10 km^2, and 20 basins with mean drainage area of 5 km^2. The basins were identified to ensure the sampling of the whole range of solar radiation characteristics of the main basin. The model was implemented to these basins by modifying only those model parameters which depend explicitly on the area and the topography of the basin, including, of course, the distribution of the radiation index. The other model parameters were transposed from those identified for the basin closed at S. Giorgio Aurino. In these comparisons, we analysed only the effect of varying the number of radiation classes. We considered only three subdivisions for the radiation classes: 1, 10 and ~~computational efficiency.~~ 20 classes, and we used the runoff obtained by using the finest spatial resolution (20 classes) as a reference against which the other two were constrasted. We used a period of four weeks (W4) as the temporal aggregation. As a matter of fact, the simulations from the model set-up W4C1 and W4C10 were compared with the corresponding simulations from the model set-up W4C20. The NSE statistics were computed only over the March. 1 to June, 30 period, i.e. the melting season. The results, reported in Table 3 as an average value of the NSE statistic over the different basins, show clearly the control exerted by the catchment size on the effect of using a different number of radiation classes for runoff simulations. The differences between W4C1 and W4C20 runoff simulations are considerable (NSE=0.77) for 5 km^2 area and rapidly decrease with increasing the drainage area. At 10 km^2 and at 20 km^2 NSE amounts to 0.91 and to 0.99, respectively. On the other hand, no degradation is reported for runoff simulated by using 10 radiation classes instead of 20, at least for drainage areas equal or exceeding 5 km^2.

5 Conclusions

This paper presents TOPMELT, a parsimonious snowpack simulation model which integrates an enhanced temperature index model into a ~~lumped~~ semi-distributed basin scale hydrological model. This is obtained by ~~describing~~ discretising the full spatial

Table 2. Nash-Sutcliffe index (NSE) of the TOPMELT-ICHYMOD model at different spatial aggregation and temporal resolution, from October 2001 to October 2007.

W4C1	**W4C5**	**W4C10**	**W4C15**	**W4C20**
0.73	0.73	0.71	0.73	0.73
W1C10	**W2C10**	**W4C10**	**W8C10**	**W12C10**
0.71	0.71	0.71	0.70	0.71

Table 3. Mean value of the Nash-Sutcliffe index (NSE) of the comparison between W4C1 and W4C10 TOPMELT-ICHYMOD simulated flows and the reference flow simulations, obtained by using the W4C20 set up, over basins of three different drainage areas: 5, 10 and 20 km^2. Comparisons carried out over the March, 1 to June, 30 period.

Model set-up	**Sub-basin area**		
	5 km^2	10 km^2	20 km^2
W4C1	0.77	0.91	0.99
W4C10	0.97	0.99	0.99

distribution of clear sky potential solar radiation ~~by means of a statistical representation, implemented by discretising the area in each elevation band~~ into a number of radiation classes ~~. Snowpack simulation~~ in each elevation band. Snowpack suimulation is carried out for each radiation class, rather than for each DTM pixel. ~~When only one radiation class for each elevation band is used, TOPMELT approximates a classical temperature-index model, whereas it approximates a fully distributed model with increasing the number of the radiation.~~ This allows to develop synthesis in modelling approaches to snow simulation and provides the potential for analysing the impact of spatial and temporal aggregation of radiation fluxes on model results. Furthermore, this approach reduces computational burden, which is a key potential advantage when parameter sensitivity and uncertainty estimation procedures are carried out.

~~Given the temporal variability of clear sky radiation distribution, the model includes a routine which ensures a consistent temporal simulation of the snow mass balance.~~ The impact of temporal and spatial aggregation of the radiation fluxes on model results is assessed by applying TOPMELT on the 614 km^2 Aurino river basin at S. Giorgio, in the Eastern Italian Alps. The analysis is carried out by examining five temporal aggregation levels (ranging from one to twelve weeks) and five spatial aggregation levels (obtained by subdividing each elevation band into a number of radiation classes ranging from one to twenty), with their impact on the prediction of snow water equivalent distribution ~~. The assessment~~ and runoff response.

The assessment of the snow water equivalent simulations clearly shows the degradation of model results when using large temporal and spatial aggregation scales, with a model efficiency decreasing up to 20%. On the other hand, ~~.~~the sensitivity analysis shows that averaging out the radiation index over four weeks and using a ten radiation classes subdivision, has a minimal impact on model results.

~~Future research will examine the scale dependency of the impact of~~ Analysis of the runoff response simulations shows that the effects of the spatial patterns of snow water equivalent are strongly smoothed at the scale of Aurino basin at S. Giorgio, with minimal deviations over the different considered model set-up. Examination of TOPMELT-driven runoff results obtained over internal sub-basins ranging in area from 5 to 20 km^2 highlight that the effects of space-time aggregation ~~on TOPMELT-driven runoff simulation, by contrasting small basins (with predominant aspects) and larger basins (where aspects become uncorrelated), and how this~~ of the solar radiation patterns on the runoff response are scale dependent, and that scale dependency is controlled by the spatial aggregation of radiation index. Simulations obtained by using just one radiation class degrade in accuracy when the model is applied over basins of around 5 km^2, whereas runoff simulations obtained with using ten radiation classes show very limited degration over all the basin areas considered. These results are important to drive implementation of TOPMELT for operational applications. They may prove relevant for ~~the~~ data-assimilation of remotely-sensed snow cover information, which may be made more effective with incresing the accuracy of the modelled snow cover. They may prove relavant also to use the spatial transferability of enhanced temperature-index model parameters to ungauged basins.

One important implication of our results concerns the transferability of the simpler temperature-index model, which is simulated in our cases when TOPMELT is implemented by using just one radiation class. The results suggest that this spatial aggregation of the radiaton patterns do not impair the spatial transferability of temperature-index models for runoff simulations of basins larger than a certain threshold, equal to 5 km^2 in our case study.

Code availability. TOPMELT is developed in Python, version 3.6, and additionally tested with Python 2.7 (Python Software Foundation, https://www.python.org/). Python installation requires the following additional modules: datetime, inspect, math, os, sys, pyodbc. The code requires the installation of a SQL database (DB) to store input data and to collects output. TOPMELT was developed and tested with MySQL Community Server (GPL), version 5.7.21. TOPMELT source code and a quick user guide are available at the repository http://doi.org/10.5281/zenodo.1342731.

References

Abudu, S., Sheng, Z., Cui, C., Saydi, M., Sabzi, H.-Z. and King, J. P.: Integration of aspect and slope in snowmelt runoff modeling in a mountain watershed, Water Sci. Eng., 9(4), 265–273, doi:10.1016/J.WSE.2016.07.002, 2016.

Anderson, E.A.: A Point Energy And Mass Balance Model of a Snow Cover. Silver Spring, Md.: U.S. Dept. of Commerce, National Oceanic and Atmospheric Administration, National Weather Service, Office of Hydrology, 1976.

Anslow, F. S., Hostetler, S., Bidlake, W. R. and Clark, P. U.: Distributed energy balance modeling of South Cascade Glacier, Washington and assessment of model uncertainty, J. Geophys. Res., 113(F2), F02019, doi:10.1029/2007JF000850, 2008.

Armstrong, R. L., Richard L. and Brun, E.: Snow and climate: physical processes, surface energy exchange and modeling, Cambridge University Press., ISBN: 9780521 854542, 2008.

Avanzi, F., De Michele, C., Morin, S., Carmagnola, C. M., Ghezzi, A. and Lejeune, Y.: Model complexity and data requirements in snow hydrology: seeking a balance in practical applications, Hydrol. Process., 30(13), 2106–2118, doi:10.1002/hyp.10782, 2016.

Borga M. and Vizzaccaro A.: On the interpolation of hydrologic variables: formal equivalence of multiquadratic surface fitting and kriging, J. Hydrol., vol. 195, no. 1–4, pp. 160–171, doi:10.1016/S0022-1694(96)03250-7, 1997.

Brock, B. W., Willis, I. C. and Sharp, M. J.: Measurement and parameterization of albedo variations at Haut Glacier d'Arolla, Switzerland, J. Glaciol., 46(155), 675–688, doi:10.3189/172756500781832675, 2000.

Carenzo, M., Pellicciotti, F., Rimkus, S. and Burlando, P.: Assessing the transferability and robustness of an enhanced temperature-index glacier-melt model, J. Glaciol., 55(190), 258–274, doi:10.3189/002214309788608804, 2009.

Carturan, L., Cazorzi, F. and Dalla Fontana, G.: Distributed mass-balance modelling on two neighbouring glaciers in Ortles-Cevedale, Italy, from 2004 to 2009, J. Glaciol., 58(209), 467–486, doi:10.3189/2012JoG11J111, 2012.

Cazorzi, F. and Dalla Fontana, G.: Snowmelt modelling by combining air temperature and a distributed radiation index, J. Hydrol., 181(1–4), 169–187, doi:10.1016/0022-1694(95)02913-3, 1996.

Comola, F., Schaefli, B., Da Ronco, P., Botter, G., Bavay, M., Rinaldo, A., and Lehning, M.: Scale-dependent effects of solar radiation patterns on the snow-dominated hydrologic response, Geophys. Res. Lett., 42, 3895–3902, doi:10.1002/2015, 2015.

Da Ros, D. and Borga, M.: Use of digital elevation model data for the derivation of the geomorphological instantaneous unit hydrograph, Hydrol. Process., 11: 13-33, doi:10.1002/(SICI)1099-1085(199701)11:1<13::AID-HYP400>3.0.CO;2-M, 1997

Dubayah, R., Dozier, J. and Davis, F. W.: Topographic distribution of clear-sky radiation over the Konza Prairie, Kansas, Water Resour. Res., 26(4), 679–690, doi:10.1029/WR026i004p00679, 1990.

Duffie, J. A. and Beckman, W. A.: Solar engineering of thermal processes, Wiley. doi: 10.1016/0038-092X(90)90061-G, 2013.

Essery, R., Morin, S., Lejeune, Y. and B Ménard, C.: A comparison of 1701 snow models using observations from an alpine site, Adv. Water Resour., 55, 131–148, doi:10.1016/J.ADVWATRES.2012.07.013, 2013.

Formetta, G., Kampf, S. K., David, O. and Rigon, R.: Snow water equivalent modeling components in NewAge-JGrass, Geosci. Model Dev., 7(3), 725–736, doi:10.5194/gmd-7-725-2014, 2014.

Hargreaves, G.H. and Samani, Z.A.: Estimating potential evapotranspiration. Journal of Irrigation and Drainage Engineering, 108, 223-230, 1982.

Hock, R. and Holmgren, B.: A distributed surface energy-balance model for complex topography and its application to Storglaciären, Sweden, J. Glaciol., 51(172), 25–36, doi:10.3189/172756505781829566, 2005.

Hock, R.: A distributed temperature-index ice- and snowmelt model including potential direct solar radiation, J. Glaciol., 45(149), 101–111, doi:10.1017/S0022143000003087, 1999.

Jóhannesson, T., Sigurdsson, O., Laumann, T. and Kennett, M.: Degree-day glacier mass-balance modelling with applications to glaciers in Iceland, Norway and Greenland, J. Glaciol., 41(138), 345–358, doi:10.3189/S0022143000016221, 1995.

Konz, M. and Seibert, J.: On the value of glacier mass balances for hydrological model calibration, J. Hydrol., 385(1–4), 238–246, doi:10.1016/J.JHYDROL.2010.02.025, 2010.

Klok, E.J., Jasper, K., Roelofsma, K.P., Gurtz J. and Badoux, A.: Distributed hydrological modelling of a heavily glaciated Alpine river basin, Hydrol. Sci. J., vol. 46, no. 4, pp. 553–570, doi:10.1080/02626660109492850, 2001.

Lee, R.: Forest microclimatology, Columbia University Press. ISBN: 9780231041560, 1978.

Li, X., Williams, M.W: Snowmelt runoff modelling in an arid mountain watershed, Tarim Basin, China. Hydrological Processes, 22(19), 3931-3940, doi:10.1002/hyp.7098, 2008.

Magnusson, J., Wever, N., Essery, R., Helbig, N., Winstral, A. and Jonas, T.: Evaluating snow models with varying process representations for hydrological applications, Water Resour. Res., 51(4), 2707–2723, doi:10.1002/2014WR016498, 2015.

Moore, R. J.: The PDM rainfall-runoff model, Hydrol. Earth Syst. Sci., 11(1), 483–499, doi:10.5194/hess-11-483-2007, 2007.

Norbiato D., Borga M., Degli Esposti S., Gaume E., and Anquetin S., Flash flood warning based on rainfall thresholds and soil moisture conditions: An assessment for gauged and ungauged basins, J. Hydrol., vol. 362, no. 3–4, pp. 274–290, 2008.

Norbiato, D., Borga, M., Merz, R., Blöschl, G. and Carton, A.: Controls on event runoff coefficients in the eastern Italian Alps, J. Hydrol., 375(3–4), 312–325, doi:10.1016/J.JHYDROL.2009.06.044, 2009.

Notarnicola, C., Duguay, M., Moelg, N., Schellenberger, T., Tetzlaff, A., Monsorno, R., Costa, A., Steurer, C. and Zebisch, M.: Snow Cover Maps from MODIS Images at 250 m Resolution, Part 1: Algorithm Description, Remote Sens., 5(1), 110–126, doi:10.3390/rs5010110, 2013.

Moore R. J. , The PDM rainfall-runoff model, Hydrol. Earth Syst. Sci., vol. 11, no. 1, pp. 483–499, 2007.

Notarnicola, C., Duguay, M., Moelg, N., Schellenberger, T., Tetzlaff, A., Monsorno, R., Costa, A., Steurer, C. and Zebisch, M.: Snow Cover Maps from MODIS Images at 250 m Resolution, Part 2: Validation, Remote Sens., 5(4), 1568–1587, doi:10.3390/rs5041568, 2013.

Oke, T. R.: Boundary layer climates, Routledge. ISBN: 9780415043199, 1992.

Orgill, J. F. and Hollands, K. G. T.: Correlation equation for hourly diffuse radiation on a horizontal surface, Sol. Energy, 19(4), 357–359, doi:10.1016/0038-092X(77)90006-8, 1977.

Östrem, G.: Ice Melting under a Thin Layer of Moraine, and the Existence of Ice Cores in Moraine Ridges, Geogr. Ann., 41, 228–230, doi:10.2307/4626805, ~~1959.~~ 1959

Parajka, J., and Blöschl, G.: Spatio-temporal combination of MODIS images - potential for snow cover mapping, Water Resour. Res.,44, W03406, doi:10.1029/2007WR006204, 2008.

Parajka, J., Holko, L., Kostka, Z. and Blöschl, G.: MODIS snow cover mapping accuracy in a small mountain catchment – comparison between open and forest sites, Hydrol. Earth Syst. Sci, 16, 2365–2377, doi:10.5194/hess-16-2365-2012, 2012.

Pellicciotti, F., Brock, B., Strasser, U., Burlando, P., Funk, M. and Corripio, J.: An enhanced temperature-index glacier melt model including the shortwave radiation balance: development and testing for Haut Glacier d'Arolla, Switzerland, J. Glaciol., 51(175), 573–587, doi:10.3189/172756505781829124, 2005.

Ranzi, R. and Rosso, R.: A physically based approach to modelling distributed snowmelt in a small alpine catchment, IAHS Publ. 205: 141-150, 1991.

Swift, L. W.: Algorithm for solar radiation on mountain slopes, Water Resour. Res., 12(1), 108–112, doi:10.1029/WR012i001p00108, 1976.

Tuo, Y., Duan, Z., Disse, M. and Chiogna, G.: Evaluation of precipitation input for SWAT modeling in Alpine catchment: A case study in the Adige river basin (Italy), Sci. Total Environ., 573, 66–82, doi:10.1016/J.SCITOTENV.2016.08.034, 2016.

Vionnet, V., Brun, E., Morin, S., Boone, A., Faroux, S., Le Moigne, P., Martin, E. and Willemet, J.-M.: The detailed snowpack scheme Crocus and its implementation in SURFEX v7.2, Geosci. Model Dev., 5(3), 773–791, doi:10.5194/gmd-5-773-2012, 2012.

Zappa, M. and Pos, F. and Strasser, U., Warmerdam, P. and Gurtz, J.: Seasonal Water Balance of an Alpine Catchment as Evaluated by Different Methods for Spatially Distributed Snowmelt Modelling, Hydrol. Rese., vol. 34, no. 3, pp. 179–202, doi:10.2166/nh.2003.0003, 2003.

Zappa M. :Objective quantitative spatial verification of distributed snow cover simulations – an experiment for entire Switzerland. Hydrological Sciences Journal, 53(1): 179–191. doi: 10.1623/hysj.53.1.179, 2008.